UNIVERSITY OF CALIFORNIA SAN DIEGO

Novel Fluorescent Guanine Analogs as Guanine Deaminase Substrates and Inhibitors

A thesis submitted in partial satisfaction of the requirements for the degree

Master of Science

in

Chemistry

by

You Wu

Committee in charge:

    Professor Yitzhak Tor, Chair
    Professor Seth Cohen
    Professor Emmanuel Theodorakis

2018

The Thesis of You Wu is approved, and it is acceptable in quality and form for publication on microfilm and electronically:

_____

_____

_____

Chair

University of California San Diego

2018

Table of Content

List of Figures

List of tables

List of Graphs

Acknowledgements

I would like to thank Professor Yitzhak Tor for providing the insight and resources for the project, teaching me to proactively think and analyze questions, encouraging me to be a better researcher. I would like to thank Andrea Fin for providing the xanthine analogues used throughout this project and teaching me how to use appropriate techniques for research. I would like to thank Paul Ludford for helping me solve the problems and overcome difficulties I meet during the project. I would like to thank all visiting members and all lab members of the Tor lab for providing advice and always supporting me.

ABSTRACT OF THE THESIS

Novel Fluorescent Guanine Analogs as Guanine deaminase substrates/inhibitors

by

You Wu

Master of Science in Chemistry

University of California San Diego, 2018

Professor Yitzhak Tor, Chair

Two fluorescent guanine analogues (thG, ^{tz}G) derived from thieno[3,4-d]-pyrimidine and isothiazole[4,3-d]-pyrimidine, respectively were synthesized and analyzed for their isomorphism and isofunction as the natural occurring guanine. Photophysical analysis demonstrated the promoted properties, such as visible emission, high quantum yield, sensitivity to polarity and pH, while the enzymatic conversion illustrated the highly isofunctional of ^{tz}G as guanine through its rapid reactivity with guanine deaminase (GDA) as the native substrate, which makes ^{tz}G be a good surrogate to help monitor the activity of GDA and assist the research for this significant enzyme in neuronal recovery.

1. Introduction

GDA is the abbreviation of guanine deaminase which can convert guanine to xanthine through a hydrolytic deamination.[1-3] It is an important metalloenzyme due to its correlations with neuronal recovery.[4] First, the conversion from guanine to xanthine is necessary for forming the dendritic spines and consequently benefits the proper brain development.[5, 6] Furthermore, GDA performs one of the steps of purine salvage pathway, which finally produces uric acid, an important antioxidant correlated with neuronal recovery and help reduce the damage from traumatic brain injury, stroke, and spinal cord injury.[3, 7, 8] At the circuit level, overexpression of GDA plays significant roles in shaping neuronal circuits and regulating the synaptic plasticity, confers resistance to neuronal death after traumatic brain injury, which makes it be one of the most significant current treatments for neurological disease.[9, 10, 11] These relations all support the significance of GDA in neurology. In addition, it is also reported that GDA is correlated with liver function while a high level of GDA activity is observed during liver diseases and transplant rejection.[12]

These significant correlations make GDA become a potentially attractive drug target for the treatment of cognitive disorder, liver diseases and purine metabolism deficiency. As a result, it facilitates the research of GDA and also the identification of its novel activator and inhibitors. However, the effective and accurate methods used to monitor the activity of GDA has not been extensively investigated.[13]

Absorbance technique is currently used for detecting the activity of GDA, but there

are a number of disadvantages for this method. First, the absorbance spectra may not be accurate enough due to the absorbance of solvent and protein, which usually absorb around 260 nm. Second, the low concentration of substrate in the enzymatic reaction results in the noise in the absorbance spectra and makes it more inaccurate. Therefore, a fluorescence technique, which is better than absorbance, was introduced here. The detection of fluorescence is much more sensitive than absorbance with less noise and it would not be influenced by solvent and non-emissive protein.

To monitor the activity of GDA by fluorescence technique, a fluorescent substrate of GDA needs to be generated, however, it's not easy to obtain good fluorescent surrogates. Generally, the structural resemblance, photophysical properties improvement and biochemical compatibility need to be considered together.[13] First, the analogues require a structural similarity to the natural counterparts, such as similar H-bonding pattern and comparable molecular size, which allows the analogues to bind to the enzyme with high specificity. Second, improved physicochemical properties than the native substrate, such as red-shifted absorbance, additional fluorescence properties and sufficient quantum yield, make the analog a more valuable alternative. Finally, the analog needs to have the same or at least similar biochemical activity as the natural substrate since the analogues are intended to be used as surrogates in the research of enzymatic reactions.

Structural compatibility plays an significant role in creating the guanine analogues.[1, 2] The size of guanine analogues should be similar as the native guanine since the overlarge substrate will result in steric clash and consequently prevent the closure of C-terminal loop, which has been reported to be necessary for the completion of the enzymatic reaction.[12]

Secondly, it's reported that correct binding between substrate and GDA ensure the stabilization of the substrate at the appropriate location in the active site in preparation for the subsequent deamination process.[13, 15, 16, 17] Therefore, the guanine analogues should also have the same binding ability as native guanine with GDA (Figure 1).
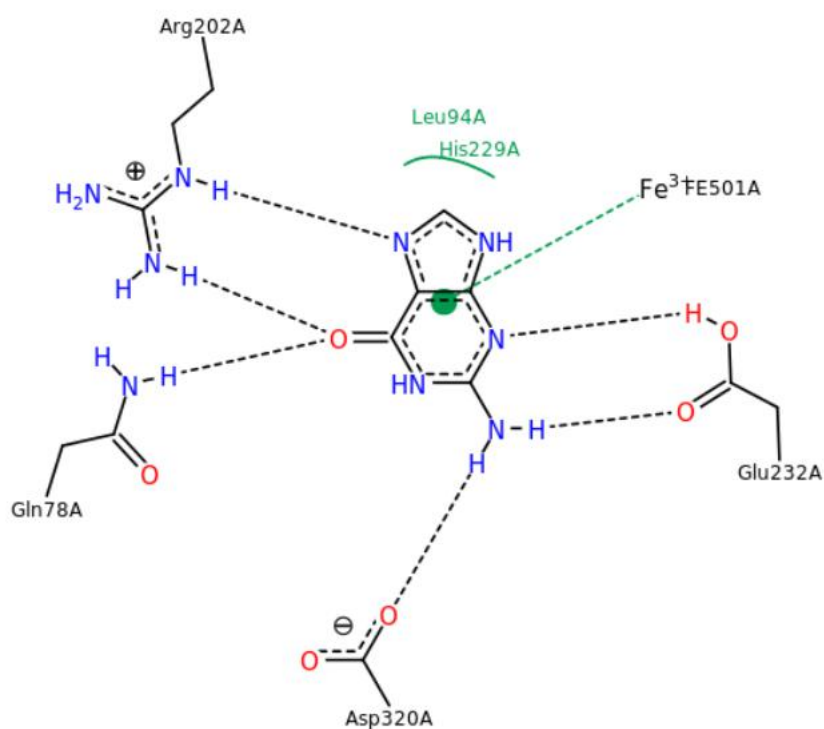
Figure 1. Crystal Structure of Guanine Deaminase from C. acetobutylicum with bound guanine in the active site[17]

Moreover, the significance of structural similarity between guanine and the analogues can also be seen from the mechanism of the enzymatic reaction.[18] As a metalloenzyme, GDA converts the guanine to xanthine through a hydrolytic deamination while the zinc atom activates the catalytic water molecule that is coordinated to the carboxylate group and generated hydroxide nucleophile.[18] It then attacks the C2 atom adjacent to the amino group resulting in the formation of a tetrahedral intermediate.[13, 17, 18] The carboxylate groups act as

the proton shuttle assist the formation of the tetrahedral structure and the collapse of this intermediate, which promotes the completion of the deamination process (Figure 2).[13, 15] Thus, the target amino group of guanine analogues should be in close proximity to the Zn atom, activated water and the carboxylate groups, and the neighbor N should be retained to support the forming of tetrahedral structure, which all ensure the ability to react with GDA.
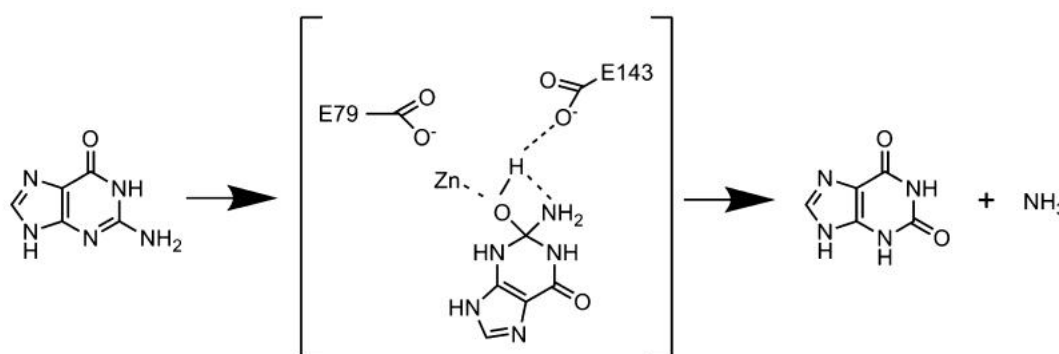
Figure 2. Reactions Catalyzed by Guanine Deaminase from Nitrosomonas europaea (NE0047) [13]

Based on the discussion above, two fluorescent guanine analogs, derived from thieno [3,4-d]-pyrimidine (thG) and isothiazole [4,3-d]-pyrimidine (^{tz}G), respectively, have been synthesized (Figure 3).[19- 24] Both of these analogues have similar structure and size compared to the native guanine, which make them have the possibility to be the surrogate of native guanine and react with GDA.[25] However, the thG may not have the similar activity as guanine due to the lack of the binding between N7 and protein.[26- 28] Further photochemical tests is performed to show their improved photophysical properties than guanine. In order to understand their biochemical reactivity with GDA, both analogs and guanine were reacted with GDA under same conditions for comparation.[29]
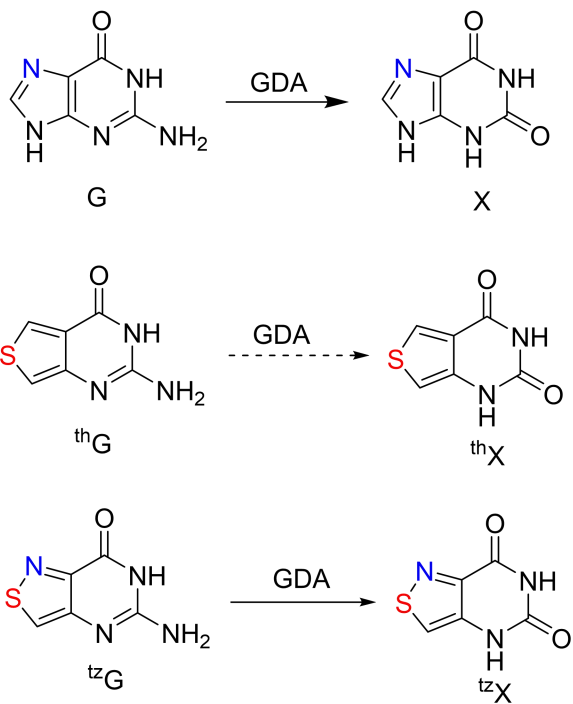
Figure 3. Enzymatic conversion of G, thG and ^{tz}G

2. Synthesis of the Nucleobases analogues.

2.1. Synthesis of thG and thX

The aminothiophene carboxylate **3** is the key precursor for synthesizing both thieno-Guanine (thG) and thieno-Xanthine (thX) through 1 and 2 steps, respectively. The synthesis of thG was accomplished through the cyclization with carbamimidic chloride. Synthesis of thX was started with the treatment of KOCN and furnished **10**, which was subjected to a nucleophilic acyl substitution to give final product thX (Figure 2).
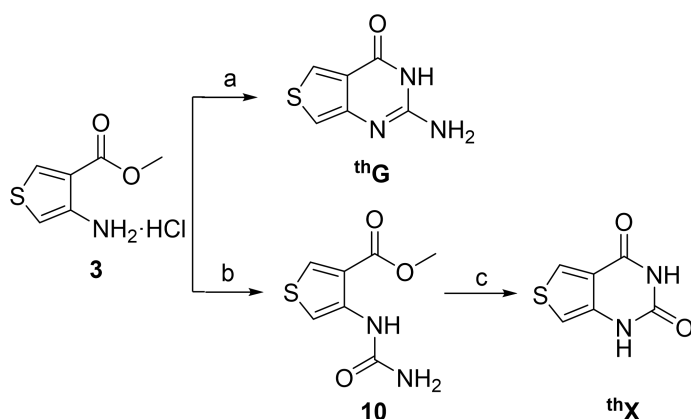
Figure 4. Synthesis of thG and thX. (a) DMSO$_2$, H$_2$O, 125°C, 1.5h, 76% (b) KOCN, H$_2$O, Acetic Acid, rt, overnight, 82%. (c) MeOH, NaOMe, rt, 16h, 74%.

2.2. Synthesis of ^{tz}G and ^{tz}X

The synthesis of two analogs of Guanine (^{tz}G) and Xanthine (^{tz}X) was started from 2-cyanoacetamide **4** through 6 and 7 steps, respectively. As a key precusor for the synthesis of both ^{tz}G and ^{tz}X, the intermediate isothiazole-core derivative **9** which is the key precursor for the synthesis of ^{tz}G and ^{tz}X, a carbamoylisothiazole carboxylate **7** was synthesized,

starting from 2-Cyanoacetamide, which was treated with sodium nitrite to give **5**. Futher reaction with tosyl chloride furnished a tosyl cyanide, which was reacted with Methyl-thioglycolate to give the isothiazole-core derivative **7**. After treatment with hydrochloride acid and a esterification reaction, **9** is given in good yield.

The isothiazole-core derivative **9** is a similar compound as **3**. With this key substrate in hand, the ^{tz}G and ^{tz}X can be yielded through the same process of forming the thG and thX from precursor **3** (Figure 3).
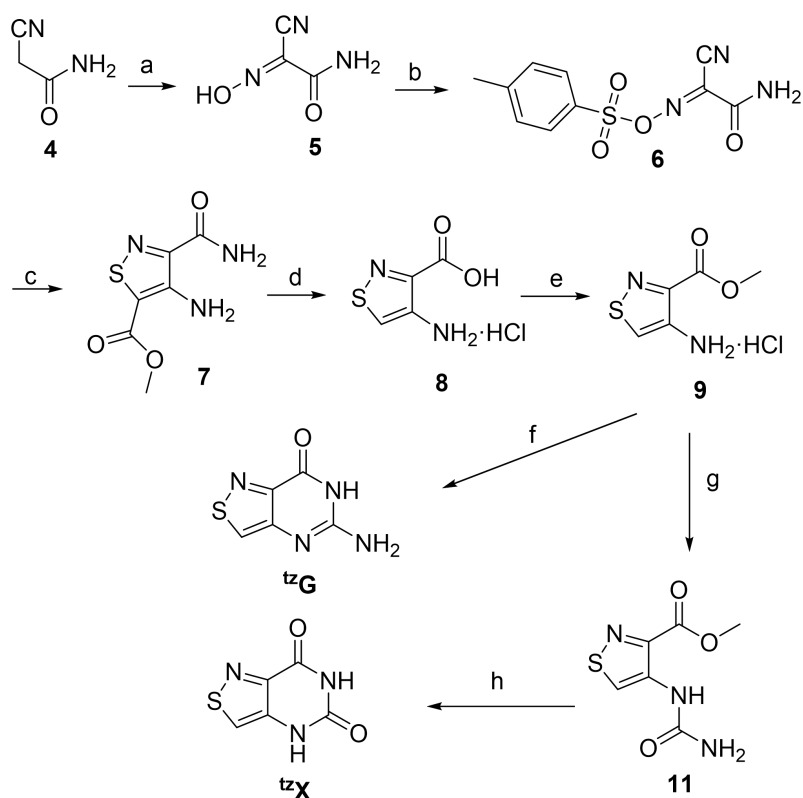
Figure 5. Synthesis of ^{tz}G and ^{tz}X. (a) NaNO$_2$, H$_2$O, Acetic Acid, 0°C, overnight, 93%. (b) TosCl, Pyridine, H$_2$O, 0°C, 2.5h, 77%. (c) Methyl-thioglycolate, EtOH, Morpholine, 0°C, 40min, 64%. (d) HCl, 110°C, 2h, 72%. (e) MeOH, H$_2$SO$_4$, NaHCO$_3$, Et$_2$O, HCl, 80°C, overnight, 69%. (f) DMSO$_2$, H$_2$O, 125°C, 1.5h, 71%. (g)KOCN, H$_2$O, Acetic Acid, rt, over night, 70%. (h) MeOH, NaOMe, rt, overnight, 94%.

2.3. Experimental methods

2.3.1. Synthesis of the nitrile precusor for the Guanine analogs preparation

NC—NH$_2$ $\xrightarrow{\text{a}}$

NH
‖
Cl $\diagup$ $\diagdown$ NH$_2$HCl

1   **2**
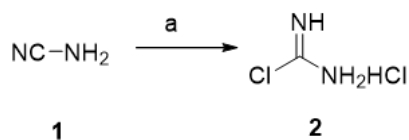
Figure 6. Synthesis of nitrile precursor 2. (a)Et$_2$O, H$_2$SO$_4$, NaCl, rt, 2h, 69%.

Synthesis of carbamimidic chloride hydrochloride (2)

3g **1** is dissolved in 200 ml Et$_2$O in a round-bottom flask. To a second round-bottom flask, H$_2$SO$_4$ is added dropwise on NaCl solid and then the generated HCl gas is directed into an empty cold trap, a water trap with H$_2$SO$_4$ for drying and an empty cold trap in order. The dried HCl flow is bubbled in the Et$_2$O solution while stirring for 2 hours. Then the formed solid is filtered on Buchner funnel and washed with Et$_2$O. After drying process under vacuum overnight, white solid is given (5.6 g, 69%).

2.3.2. Synthesis of thG

Synthesis of 2-aminothieno[3,4-d]pyrimidin-4(3H)-one (thG)

A well-mixed fine solid of **3** (1.0 g, 5.2 mmol) and **2** (0.83 g, 7.3 mmol) is dissolved to DMSO$_2$ (16.67 g) at 125 °C in a round-bottom flask over 20 minutes and is stirred for 1.5 hours for the reaction. Then the suspension is cooled to room temperature and the mixture is dissolved into 65 ml H$_2$O. After basified with NH$_2$OH to pH 10, the mixture is stirred for 1 hour. The formed creamy solid is filtered in a Buchner Funnel and washed by H$_2$O and Et$_2$O respectively. After drying under vacuum for 2 days, the yellow solid is given (0.66 g, 76%). ESI-HRMS calculated for C$_6$H$_5$N$_3$OS [M+H]$^+$ 168.0226 found 168.0226. ^{1}H NMR (300 MHz, DMSO-D6) δ 10.57 (s, 1H), 8.23 (d, J = 3.3 Hz, 1H), 6.96 (d, J = 3.3 Hz, 1H), 6.11 (s, 2H). ^{13}C NMR (126 MHz, DMSO) δ 159.78 (s), 151.61 (s), 149.78 (s), 127.67 (s), 124.26 (s),

108.84 (s).

2.3.3. Synthesis of ^{tz}G

Synthesis of 2-amino-N-hydroxy-2-oxoacetimidoyl cyanide (5)

To a 250 ml round bottom flask, **4** (10 g, 0.12 mol) and sodium nitrite (10 g, 0.15 mol) is dissolved in 100 ml H_2O at 0°C. Acetic Acid (14 ml) is added drop by drop in the mixture for 30 minutes. After stirring overnight, the product can be extracted with Ethyl Acetate and evaporate to get the white solid (13 g, 93%).

Synthesis of 2-amino-2-oxo-N-(tosyloxy)acetimidoyl cyanide (6)

To a 100 ml round bottom flask, **5** (2.5 g, 0.022 mol) is dissolved in 18 ml Pyridine (anhydrous, 99.8%) at 0 °C, and 4-methyl benzene sulfonyl chloride is added in 4 portions every 15 minutes (1.1 g x 4, 0.023 mol). 1 hour after starting adding 4-methyl benzene sulfonyl chloride, 10 ml pyridine is added into the mixture and the solution is stirred for 1 hour at 0 °C. After adding 40 ml H_2O / ice mixture, the solution is stirred for another 30 minutes and white solid is filtered in Buchner funnel and dried in vacuum overnight (4.6 g, 77%).

Synthesis of methyl 4-amino-3-carbamoylisothiazole-5-carboxylate (7)

To a 100 ml round bottom flask, **6** (2.49 g, 9.3 mmol) is dissolved in 10 ml EtOH at 0 °C and 1 ml Methyl-thioglycolate is added after preparing a well-mixed solution with 1.4 ml morpholine and 1 ml EtOH, then the mixture is added dropwise over 10 minutes into the

flask. The solution turns from white to yellow during the adding of the morpholine / EtOH mixture and the reaction is stirring for another 30 minutes at 0 °C. After consumption of **6** as monitored by TLC, 40 ml of iced water is added and the suspension is filtered to get a white solid. After drying under vacuum overnight, the product is given (1.2 g, 64%).

Synthesis of 4-aminoisothiazole-3-carboxylic acid hydrochloride (8)

To a 100 ml round bottom flask, **7** (2.5 g, 12 mmol) is dissolved in HCl (32.8 ml) and the solution is boiled at 110 °C for 2 h. After cooling down in ice bath, pink solid can be filtered (1.6 g, 72%).

Synthesis of methyl 4-aminoisothiazole-3-carboxylate hydrochloride (9)

To a 100 ml round bottom flask, **8** (1.6 g, 8.9 mmol) is dissolved in MeOH (31.7 ml) and H_2SO_4 (1.5 ml) and the solution is refluxed at 80 °C overnight. After cooling down to room temperature, $NaHCO_3$ is used to neutralize the solution to pH 4. Following with the extraction with Et_2O, and $NaSO_4$ is added to remove extra H_2O. Solvent removed by evaporation, then HCl in dioxane (4 M, 10 ml) is added to the solution and the suspension was evaporated to dryness to give **9** as yellow-brown hydrochloric salt solid (1.2 g, 69%).

Synthesis of 5-aminoisothiazolo[4,3-d]pyrimidin-7(6H)-one (^{tz}G)

A well-mixed fine solid of **9** (1.5 g, 7.7 mmol) and **2** (1.32 g, 11.6 mmol) is added slowly and dissolved in melted $DMSO_2$ (25.5 g) at 125 °C in a round-bottom flask over 20 minutes and reacting at 125 °C for 1.5 hours. Then the suspension is cooled to room

temperature and the mixture is dissolved into 120 ml H_2O. After basified with NH_2OH to pH 10, the mixture is followly stirred for 1 hour. The formed creamy solid is filtered in a Buchner funnel and washed by H_2O and Et_2O respectively. After drying under vacuum for 2 days, the yellow solid is given (0.92 g, 71%). ESI-HRMS calculated for $C_5H_4N_4OS$ $[M+H]^+$ 169.0179 found 169.0177. ^{1}H NMR (300 MHz, DMSO-D6) δ 11.06 (s, 1H), 8.62 (s, 1H), 6.32 (s, 2H). ^{13}C NMR (126 MHz, dmso) δ 156.70 (s), 151.71 (s), 150.79 (s), 149.01 (s), 136.72 (s).

2.3.4. Synthesis of [th]X

[th]X is synthesized by our lab member, Andrea Fin.

Synthesis of methyl 4-ureidothiophene-3-carboxylate (10)

3 (2 g, 10.4 mmol) is dissolved in H_2O and Acetic Acid (25 ml, 1:1 ratio) in a 100 ml round bottom flask, then KOCN (1.67 g, 20.6 mmol) is dissolved in H_2O and added dropwise to the solution at room temperature. The reaction is stirred overnight, then the mixture is filtered using the Buchner funnel and washed with H_2O. The White powder is given (1.708 g, 82%).

Synthesis of thieno[3,4-d]pyrimidine-2,4(1H,3H)-dione ([th]X)

To a round bottom flask, **10** (1 g, 5 mmol) is suspended in MeOH (10 ml), and then NaOMe (22 ml) is added slowly to the mixture. After 16 hours stirring, the milky solution is filtered and white solid is washed with MeOH (70 ml) and dried in vacuum. For more purification, the white solid is dissolved in MeOH and H_2O (1:1 ratio), and acidified with

formic acid. After stirring at room temperature for 1 hour, the white precipitate is given

(0.621 g, 74%). ESI-HRMS calculated for $C_6H_4N_2O_2S$ $[M+H]^+$ 166.9921 found 166.9922. ^1H

NMR (500 MHz, DMSO-D6) δ 10.91 (s, 2H), 8.31 (d, J = 3.2 Hz, 1H), 6.78 (d, J = 3.2 Hz,

1H). ^{13}C NMR (126 MHz, dmso) δ 159.07 (s), 151.25 (s), 138.20 (s), 130.63 (s), 122.35 (s),

103.17 (s).

2.3.5. Synthesis of ^{tz}X

^{tz}X is synthesized by our lab member, Andrea Fin.

Synthesis of methyl 4-ureidoisothiazole-3-carboxylate (11)

9 (1.0 g, 5.2 mmol) is dissolved in H_2O and Acetic Acid (20 ml, 1:1 ratio) in a 100 ml

round bottom flask, then KOCN (2.0 g, 24.7 mmol) is dissolved in H_2O and added dropwise

to the solution at room temperature. The reaction is stirred overnight, then the mixture is

filtered using the Buchner funnel and washed with H_2O(70 ml). The White powder is given

(0.73 g, 70%).

Synthesis of isothiazolo[4,3-d]pyrimidine-5,7(4H,6H)-dione (^{tz}X)

To a round bottom flask, **11** (0.710 g, 3.53 mmol) is suspended in MeOH (10 ml),

then NaOMe (15 ml) is added dropwise to the mixture and a dense and yellowish solution is

observed. After stirring over night at room temperature, the milky solution is filtered and the

yellow solid is washed with MeOH (60 ml) and dried in vacuum. For more purification, the

yellow solid is dissolved in MeOH / H_2O (1:1 ratio), and acidified with formic acid to get

white precipitate. Solution is stirred for 1 hour at room temperature, then filtered to get white

solid (0.56 g, 94%). ESI-HRMS calculated for $C_5H_3N_3O_2S$ [M+H]$^+$ 167.9873 found 167.9874.

^{1}H NMR (500 MHz, DMSO-D6) δ 11.60 (s, 1H), 11.37 (s, 1H), 8.62 (s, 1H). ^{13}C NMR (126

MHz, dmso) δ 157.02 (s), 150.81 (s), 146.94 (s), 138.50 (s), 130.74 (s).

2. Crystal Structure

Crystal structure determination confirmed the proposed structure (Figure 2) and the structural similarity between two analogues and native guanine. The existence of two structures of [th]G proves the tautomerism in the solid state of [th]G. The H-bonding between the two structures connects them through Watson-Crick face, which is the same face as the connection between guanine and cytosine, further confirmed the structural analogy between the analogue and guanine. [30, 31]
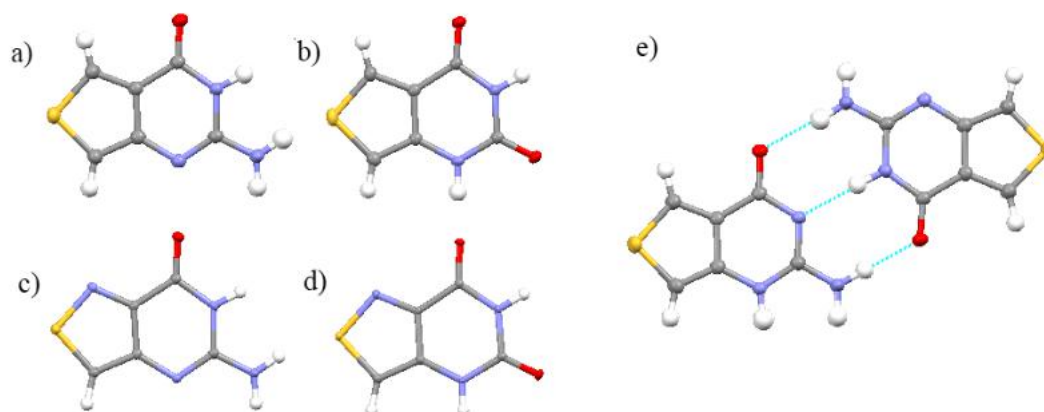
Figure 7. X-ray crystal structures of (a) [th]G, (b) [th]X, (c) [tz]G, (d) [tz]X. (e)Tautomerization of [th]G.

3. Photophysics of nucleobase analogues.

3.1. Photophysics analysis

The fundamental spectroscopic properties, including the molar absorption coefficient, quantum yield, sensitivity toward polarity, and the spectroscopically derived pK_a values of the nucleobases analogues are listed in Table 1. The red-shifted maxima of the ground-state absorption spectra is showed for the four analogues comparing to the native nucleobases, G (275 nm) and X (273 nm) (Graph 1a). The molar absorption coefficient of ^{th}G, ^{th}X, ^{tz}G, and ^{tz}X are 3.31, 3.03, 5.09, 6.13, respectively (Table 1). All Emission spectrum were excited at their maximum absorption and the maxima is observed to be ranged from 394 nm (^{tz}X) to 446 nm (^{tz}G). The emission quantum yield of the two thieno-ring analogues are 0.36 and 0.46 for ^{th}G and ^{th}X, respectively, which were higher than the two isothiazole-ring analogues, with 0.07 for ^{tz}G and 0.02 for ^{tz}X in water.

Table 1. Photophysical Properties of Guanine and Xanthine Analogues.

|	solvent	$\lambda_{abs}(\varepsilon)^a$	$\lambda_{emi}(\Phi)^a$	$\Phi\varepsilon$	Stokes shift^a	Polarity sensitivity^b	$pK_a{}^c$(abs)
thG	water	315 (3.04±0.03)	439 (0.40±0.04)	1179	8.97		4.41, 10.19
	Dioxane	325 (2.96±0.02)	423 (0.40±0.05)	1182	7.18	137.4	
thX	water	308 (3.16±0.08)	420 (0.46±0.05)	1406	8.66		3.28, 8.96
	Dioxane	303 (3.63±0.03)	383 (0.065±0.002)	242	6.95	71.9	
^{tz}G	water	320 (5.43±0.03)	446 (0.068±0.004)	351	8.88		8.80
	Dioxane	336 (5.07±0.03)	419 (0.026±0.001)	129	5.90	125.3	
^{tz}X	water	315 (6.13±0.05)	394 (0.018±0.001)	116	6.42		9.92
	Dioxane	315 (6.427±0.007)	375 (0.001±0.001)	11	5.08	53.1	

a. λ_{abs}, ε, λ_{emi}, and Stokes shift are reported in nm, $10^3 M^{-1}cm^{-1}$, nm, and $10^3 cm^{-1}$ respectively. b. Sensitivity to solvent polarity reported in $cm^{-1}/(kcal\ mol^{-1})$ is equal to the slope of the linear fit in Graph 2. c. pK_a values are equal to the inflection point determined by the fitting curves in Graph 3.
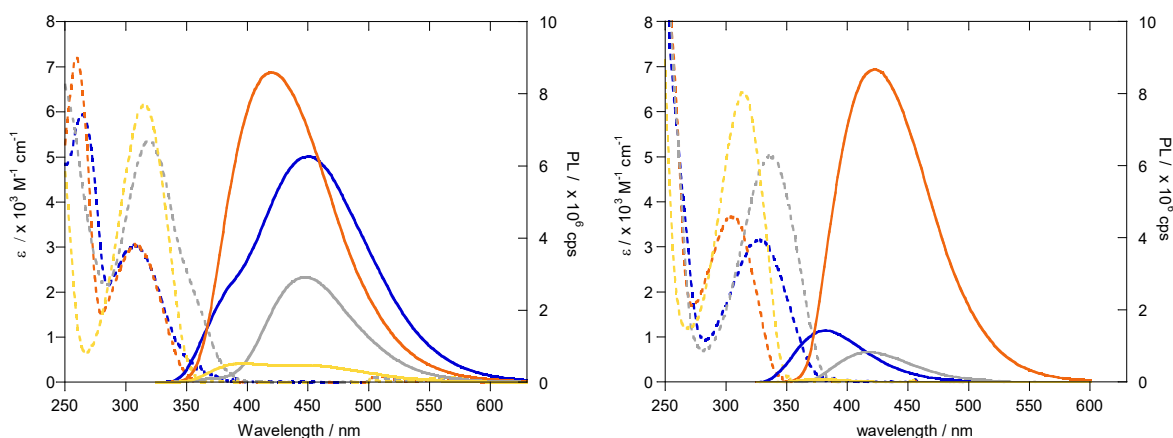
Graph 1. Emission and Absorbance spectrum for thG (blue), thX (orange), ^{tz}G (gray), ^{tz}X (yellow) in water (left) and dioxane (right).

The absorption spectra measured in dioxane showed bathochromic shifts for thG and ^{tz}G, slight hypochromic shift for thX and no significant change for ^{tz}X compared to the aqueous solutions (Graph 1b). The emission intensity of thX, ^{tz}G, ^{tz}X is obviously lower in

dioxane than in water, except ^{th}G, for which is significantly higher than in water. The fluorescence maxima displayed a remarkable hypochromic shift for all four nucleobases analogues. Quantum yield in Dioxane for ^{th}G (0.35) is higher than ^{tz}G (0.03), and are still closed to their corresponding values in water, while the quantum yield for ^{th}X is significantly lower than in water and no remarkable change for ^{tz}X. The sensitivity of the four nucleobase analogues to solvent polarity is reflected by the slope of the linear fitting between the measured Stokes shifts and microscopic solvent polarity parameters,$E_T(30)$ (Graph 2, Table 1).
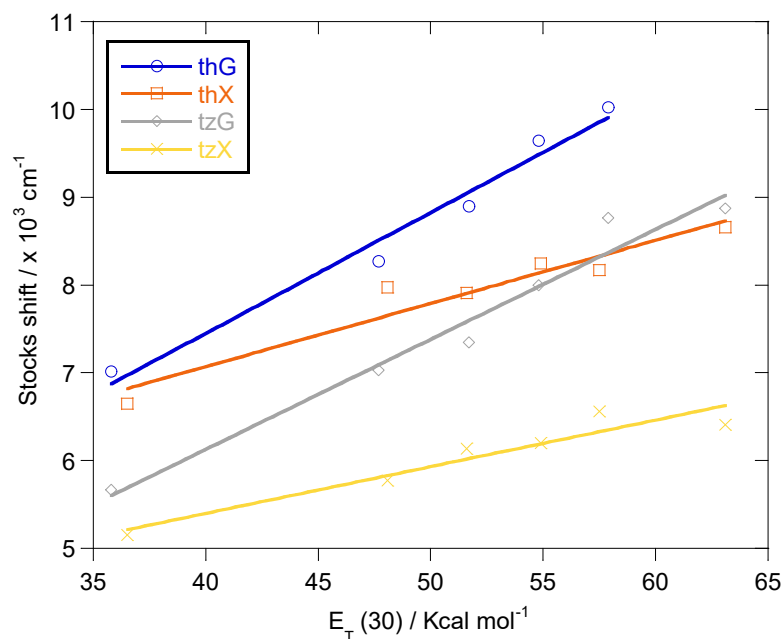
Graph 2. Stokes shift correlation versus solvent polarity ($E_T(30)$) of water/dioxane mixtures for ^{th}G (blue), ^{th}X (orange), ^{tz}G (gray) and ^{tz}X (yellow).

All nucleobase analogues display sensitivity toward pH change, as a result, the pK$_a$ values can be extracted from the dependence of the absorbance on pH (Graph 4). To exclude the influence of concentration, the graph of absorbance differences between two specific wavelengths versus pH is generated for the G analogues and X analogues (Graph 3, Table 1).

The signigicant change of absorbance characterized the pKa of these four nucleobase

analogues, yielding two pKa value for thG (4.41 and 10.19) and ^{tz}X (3.28, 8.96) and one for

^{tz}G (8.80) and ^{tz}X (9.92).
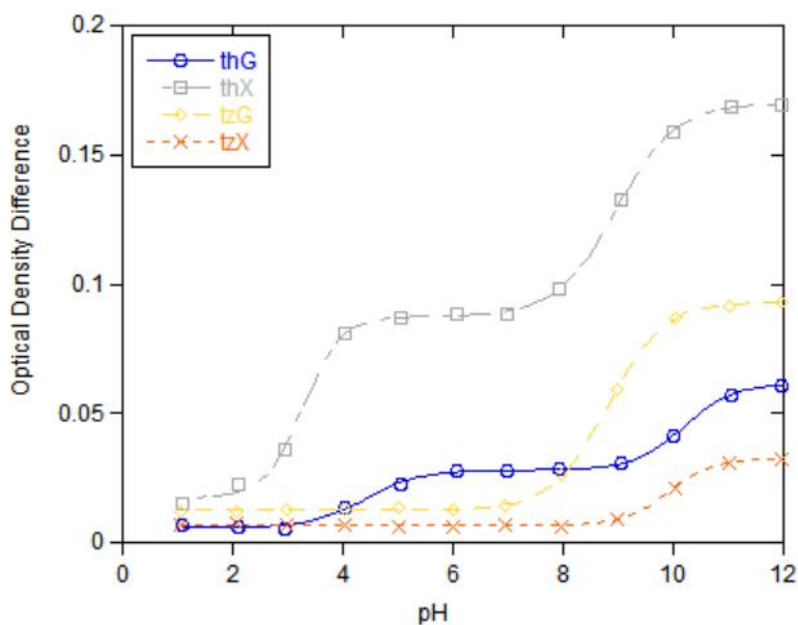
Graph 3. Optical density difference versus pH for thG, thX, ^{tz}G, and ^{tz}X.

3.2. Experimental methods

Spectroscopic grade DMSO and dioxane were obtained from Alfa Aesar and Acros

and aqueous solutions were prepared with de-ionized water. All the measurements were

carried out in a 1 cm four-sided quartz cuvette from Helma.

Absorption spectra were measured on a Shimadzu UV-2450 spectrophotometer setting

the slit at 1 nm and using a resolution of 0.5 nm. All the spectra were corrected for the blank.

Steady state emission spectra were measured on a Horiba Fluoromax-4 equipped with a

cuvette holder with a stirring system setting both the excitation and the emission slits at 3 nm,

the resolution at 1 nm. The steady state fluorescence spectra were performed upon excitation

at the wavelength of the maximum absorption.

All the spectra were corrected for the blank. Both instruments were equipped with a thermostat controlled ethylene glycol-water bath fitted to specially designed cuvette holder and the temperature was kept at $37.00 \pm 0.10 \, °C$.

Nucleobases were dissolved in DMSO to prepare highly concentrated stock solutions: X (13.15 mM), thG (11.96 mM), thX (11.89 mM), tzG (11.89 mM) and tzX (11.82 mM). G has relatively low solubility in DMSO, then G is dissolved in basic NaOH aqueous solution (pH 12) and the concentration is 11.23 mM. In a typical experiment, aliquots (10 μl) of the concentrated DMSO solution were diluted with air-saturated solvents (3 ml). The solution were mixed with a pipette for 15 seconds and placed in the cuvette holder at $37.00 \pm 0.10 \, °C$ for 3 minutes before spectra were recorded. All sample except Guanine contain 0.3 v/v % of DMSO.

3.2.1. Fluorescence quantum yield

The samples concentration were adjusted to have an optical density lower than 0.1 at the excitation wavelength (λ_{ex}). The fluorescence quantum yield (Φ) were evaluated based on an external standard, 2-aminopurine (0.68 in water, λ_{ex} 320 nm) by using the following equation.

$$\Phi = \Phi_{STD} \frac{I}{I_{STD}} \frac{OD_{STD}}{OD} \frac{n^2}{n_{STD}^2}$$

Where Φ_{STD} is the fluorescence quantum yield of the standard, I and I_{STD} are the

integrated area of the emission band of the sample and the standard respectively, OD and ODSTD are the optical density at the excitation wavelength for the sample and the standard respectively and n and nSTD are the solvent refractive index of the sample and the standard solutions respectively.

3.2.2. Sensitivity to pH

Sodium phosphate buffers (30 ml) were prepared by mixing sodium phosphate dibasic and sodium phosphate monobasic to have a final concentration of 50 mM. The pH of each solution was adjusted to the desire value by adding aliquots of 2 M aqueous HCl or 1 M aqueous NaOH prior to spectral measurements.

The absorption (λ_{abs}) difference between two selected wavelength were plotted versus the pH and fitted using a Boltzmann sigmoidal curve using Kaleidagraph 3.5 (Graph 3). The pK_a values were determined by interpolation of the fitting curves. The values and the relative standard deviations are reported in table 1.
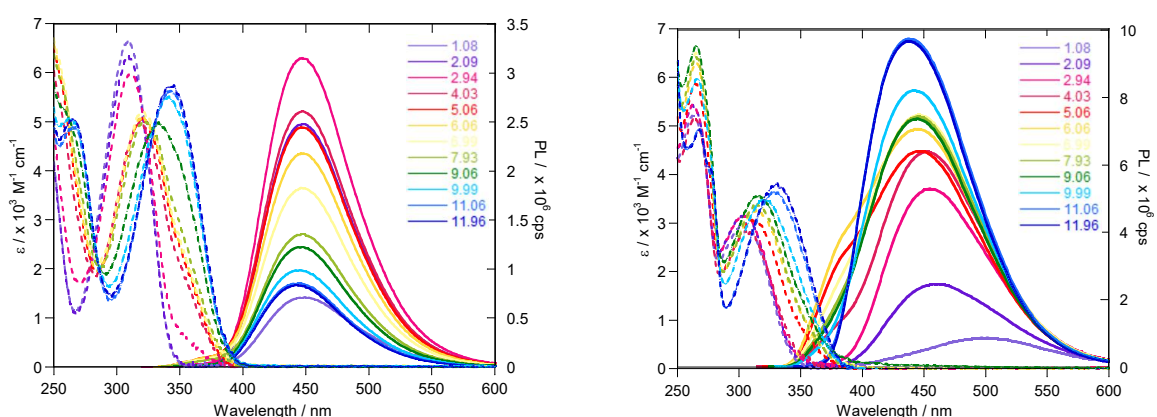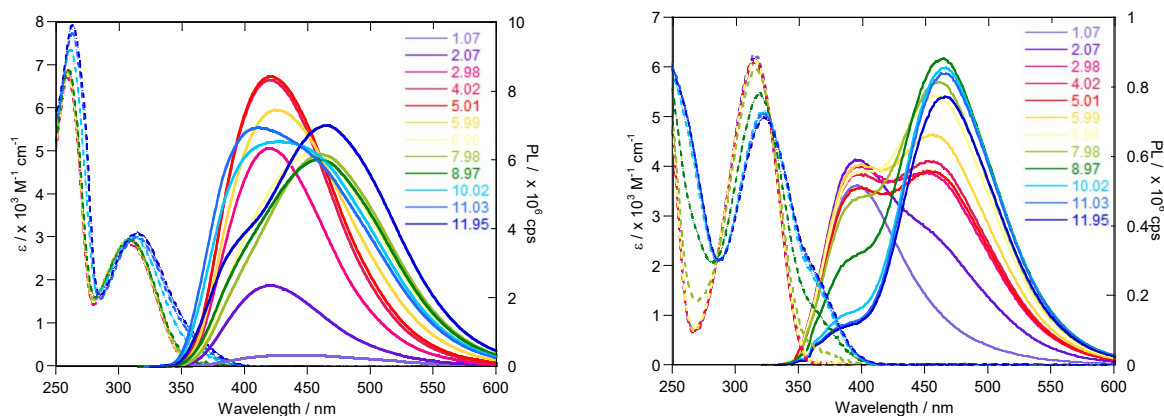
Graph 4. Absorption (dashed lines) and emission (solid lines) traces in buffer solutions at different pH for [th]G (upper left), [th]X (upper right), [tz]G (bottom left), and [tz]X (bottom right).

3.2.3. Sensitivity to polarity

Experiments evaluating the effect of polarity were performed in water, dioxane and their mixtures (20, 40, 60 and 80 v/v % water in dioxane) (Graph 5). The sample $E_T(30)$ values were determined by dissolving a small amount of Reichardt's dye in the mixture of the same solvent used to dilute the nucleobase's DMSO sample. The observed long wavelength absorption maximum (λ_{abs}^{max}) was converted to the $E_T(30)$ values with the following equation (Table 2).

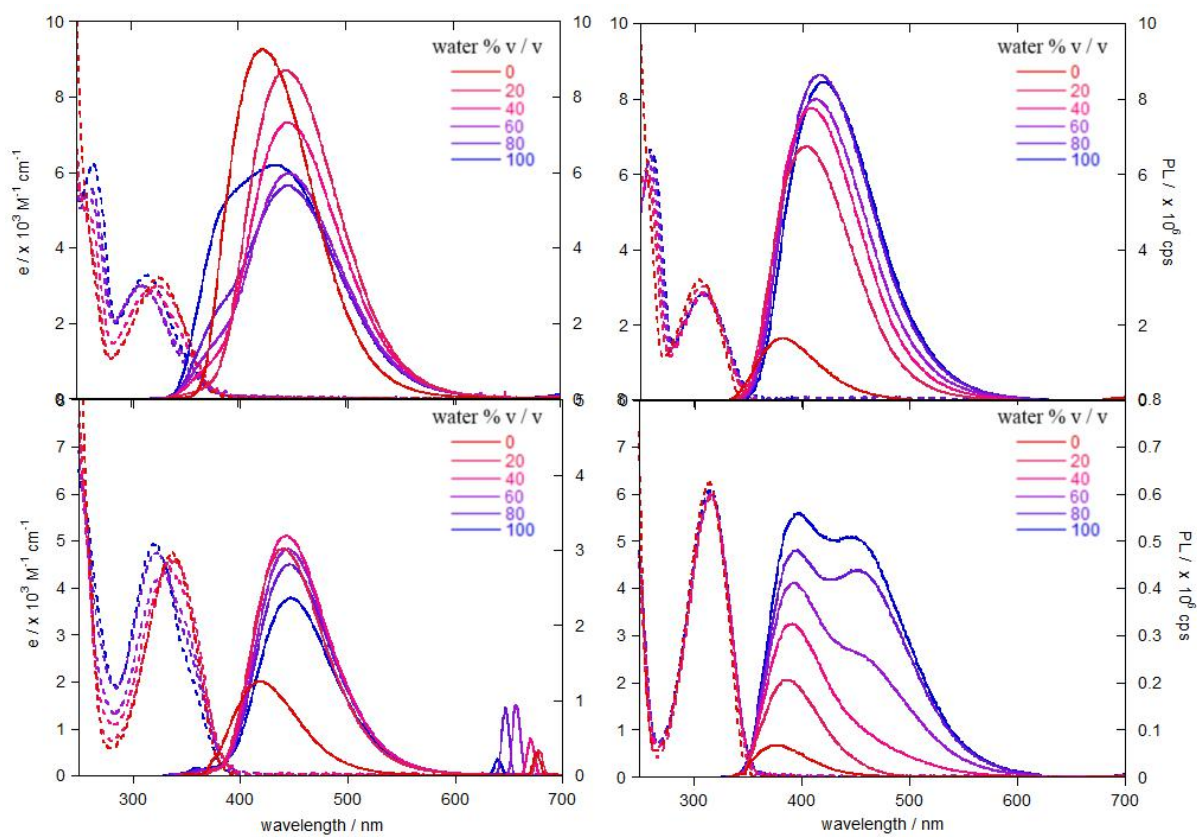$$E_T(30) = \frac{28591}{\lambda_{abs}^{max}}$$

Table 2. $E_T(30)$ experimental values for water/dioxane mixtures. Due to solubility limitation the water ET(30) value was not calculated.

Water:Dioxane	Reported $E_T(30)$ (Kcalmol^{-1})	Experimental $E_T(30)$ (Kcalmol^{-1})for [th]G and [tz]G	Experimental $E_T(30)$ (Kcalmol^{-1})for [th]X and [tz]X
1:0	63.1	-	-

4:1	57.5	57.9	57.5
3:2	55.0	54.8	54.9
2:3	51.6	51.7	51.6
1:4	48.3	47.7	48.1
0:1	36.4	35.8	36.5

Graph 5. Absorption (dashed lines) and emission (solid lines) traces in water, dioxane and mixture thereof for thG (upper left), thX (upper right), tzG (bottom left), and tzX (bottom right).

4. Enzymatic conversion from G analogue to X analogues.

4.1. Enzymatic analysis

To explore the different biochemical activity of the nucleobase analogues, guanine deaminase (GDA) was chosen to react with these potential substrates. The result can help demonstrate the utility of these fluorescent analogues and also the impact of restoring the basic N7 in the enzymatic reaction. It has been previously reported that the enzymatic conversion of a thieno-core Adenosine analogus ([th]A) to the corresponding inosine derivative ([th]I) is significantly lower than the naturally occurring adenosine.[27, 28] However, the deamination of isothiazole-core adenosine ([tz]A) to inosine ([tz]I) is at the similar rate as of A to I.[29] The H-bonding between N7 and the residue of the protein in the crystal structure of GDA further demonstrate the significance of the N7 in the reaction.[15- 17] Therefore, we hypothesized that the Guanine analogues have the similar property, which is that the [tz]G may not have higher activity than the [th]G because of the the restoring of N7.

Firstly, the reaction between GDA and [th]G was tested. Both the steady state absorption and emission didn't change much during the time after adding GDA to the [th]G, which showed that the GDA could barely react with [th]G, while the spectras taken for [tz]G showed a obvious and fast conversion from [tz]G to [tz]X (Graph 10, 11). Real-time continuous absorbance and emission were also performed relying on the photophysical differences between the reagents and expected products (Graph 12, 13, 14). The result confirmed that the GDA cannot deaminate [th]G and showed that the deamination of [tz]G to [tz]X is almost as efficient as G to X.

Assuming a first order reaction, the reaction half-life for ^{tz}G and G deamination were also calculated for comparison ($t_{1/2}$ = 33.6 ± 3.6 s for ^{tz}G and $t_{1/2}$ = 33.7 ± 3.6 s for G), which were very closed to each other. This result substantiated my hypothesis, which was further confirmed by HPLC analyses (Graph 6). In summary, the improved functionality of the ^{tz}G over the ^{tz}G was highlighted from these observations, which supported the hypothesis of the significance of the N7 in the enzymatic reaction.
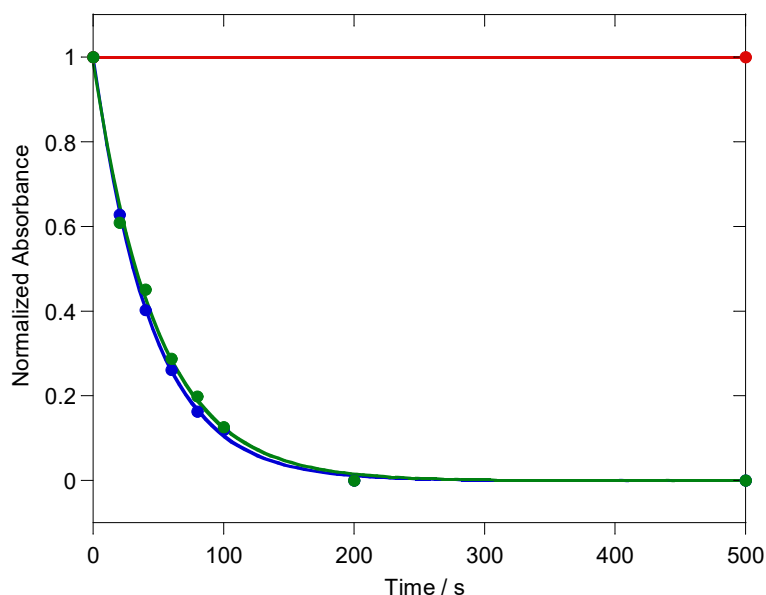
Graph 6. Normalized absorbance intensity from HPLC versus reaction time for G (blue), thG (red) and ^{tz}G (green).

Since thG cannot react with GDA, a hypothesis of being a inhibitor for the enzymatic convertion catalyzed by GDA is further presented. We selected to probe additional HPLC analyses for exploring the activity of G with the well-mixed GDA and thG. The unaffected convertion of G to X illustrated thG is neither substrate nor a inhibitor of GDA.

4.2. Experimental Methods.

Recombinant human guanine deaminase protein (GDA) was obtained from Novus Biologicals (catalog number NBP2-49692-20ug). Sodium phosphate buffer was prepared to dilute the enzyme solution 10:1 by dissolving an aliquot (2 μl) in it (18 μl, 50 mM, pH 7.5). The enzyme solution was freshly prepared and kept in ice bath prior to use.

Concentrated stock solutions in DMSO were prepared for X (6.66 mM), thG (6.09 mM), thX (6.69 mM), ^{tz}G (4.79 mM), ^{tz}X (6.54 mM) and in H$_2$O (pH 12) for G (9.85 mM). These concentrated stock solution were used for steady state absorbance and emission for clearer graphs and was diluted 20:1 for usage of kinetic measurement and HPLC traces to see the first order reaction process.

4.2.1 Steady state absorption and emission experiment in presence of GDA

Steady state absorption spectra over time were measured on a Shimadzu UV-2450 spectrophotometer setting the slit at 1 nm and using a resolution of 0.5 nm. All the spectra were corrected for the blank. Steady state emission spectra were measured on a Horiba Fluoromax-4 equipped with a cuvette holder with a stirring system, setting the excitation and the emission slits at 3 nm, the resolution at 1 nm, and excitation wavelength as it of the maximum absorbance. All the spectra were corrected for the blank.

The steady state sbsorption and emission of nucleobases (G, thG, ^{tz}G), their expected product with GDA (X, thX, ^{tz}X) and the mixture (25, 50, 75% expected products in reagents) were measured as the standard (Graph 7). The emission of G is absent since G doesn't have fluorescence property. The emission spectrums were excited at 360 nm (Graph 8).
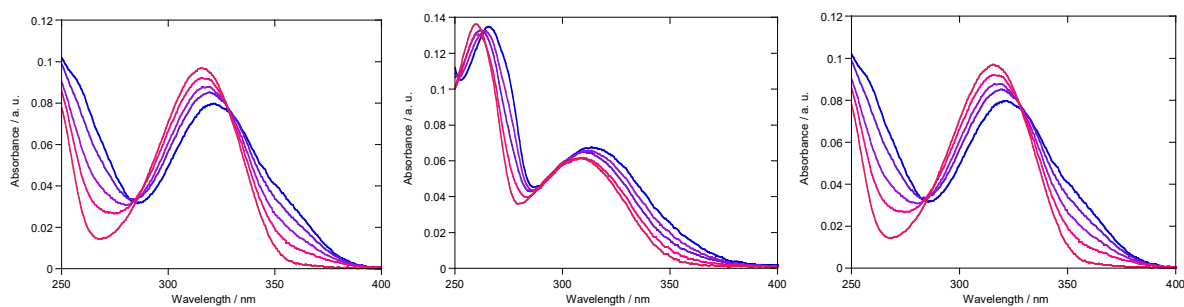
Graph 7. Absorbance trance of G, X and the mixture thereof (left); thG, thX and the mixture thereof (middle); tzG, tzX and the mixture thereof (right) in pH 7.5 Sodium Phosphate buffer at 37 °C. The color for G, thG, tzG is blue and for X, thX, tzX is red.
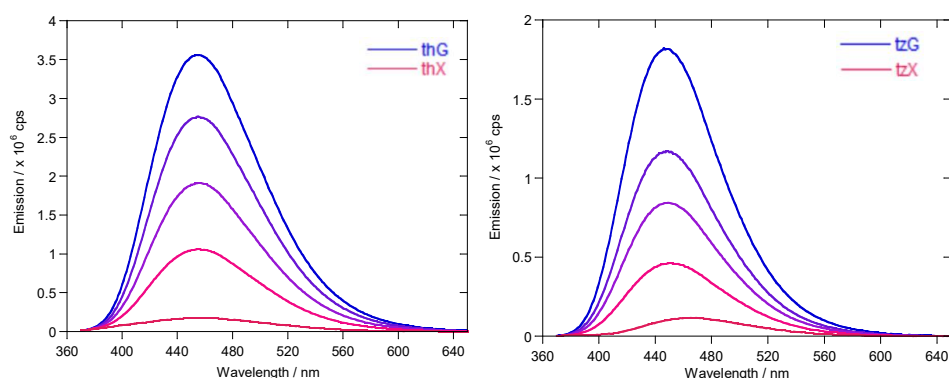
Graph 8. Emission trance of a) thG (blue), thX (red) and the mixture thereof; b) tzG (blue), tzX (red) and the mixture thereof in pH 7.5 Sodium Phosphate buffer at 37°C.

Steady state absorbance during time after the injection of GDA into G, thG and tzG in the sodium phosphate buffer (pH 7.5) at 37°C, which is in the same condition as the standard, were measured every 1 min and the absorption and emission for reagents and products were also obtained to compare with the standard (Graph 10, 11). All setting is same as the standard measurement.
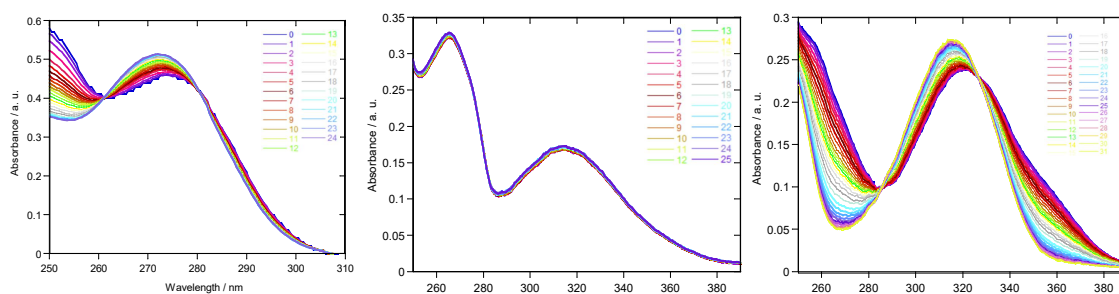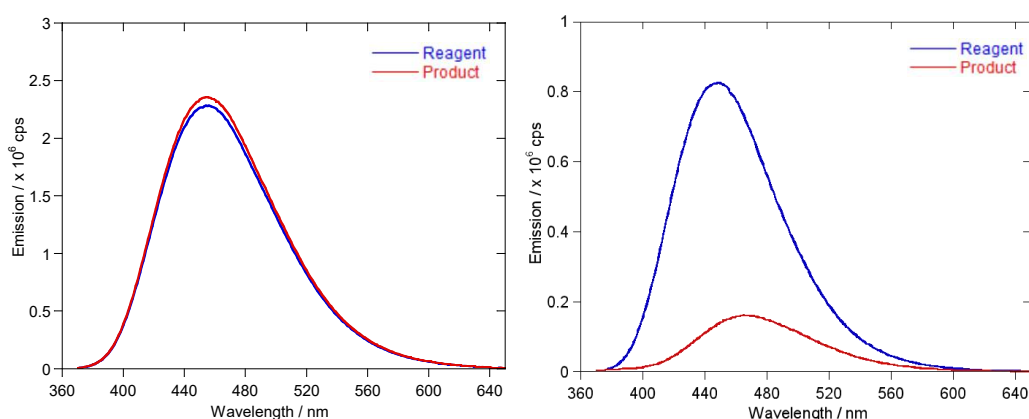

Graph 9. Steady state absorbance spectrum during the enzymatic reaction of G (left), thG (middle) and tzG

(right).
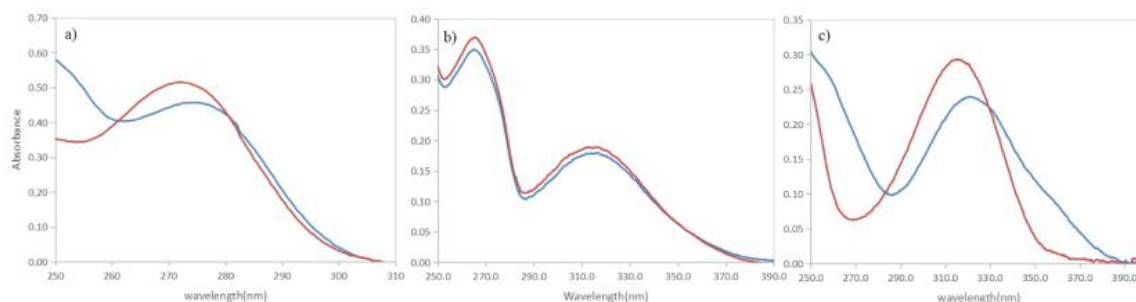
Graph 10. Absorbance spectrum of reagent (Blue) and product (red) of the enzymatic conversion of GDA with a) G; b) thG; c) ^{tz}G in pH 7.5 Sodium Phosphate buffer at 37℃.

Graph 11. Emission spectrum of reagent (Blue) and product (red) of the enzymatic conversion of GDA with a) thG; b) ^{tz}G in pH 7.5 Sodium Phosphate buffer at 37℃.

4.2.2. Absorbance and fluorescence based kinetic assays in presence of ADA

For G the ^{tz}G traces, the spectroscopy sample were prepared in 1 cm quartz cuvette from Helma to give a nucleobase and enzyme concentration of 2.00 μM and 2666 mU/ml in phosphate buffer (50 mM, pH 7.5) and were measured at $37.00\pm0.10℃$.

The ADA-mediated enzymatic conversion of guanine and the two guanine analogue were also monitored through the kinetic absorbance and emission base on the difference absorbance and emission between substrates and products at a fixed wavelength.

The enzymatic conversion for G to X was performed on a Shimadzu UV-2450 spectrophotometer setting the slit at 1 nm, taking a point every 2 seconds for total 500

seconds at 270nm upon addition of GDA.

The exzymatic conversion of [th]G to [th]X, [tz]G to [tz]G were performed on a Horiba Fluoromax-4 setting the excitation and the emission slits at 3 nm, excitation wavelength as 360 nm, measured at the wavelength of their maximum emission for every 30 s and 10 s with the total time is 1 hour and 500 seconds for [th]G and [tz]G respectively (Graph 12, 13, 14).

The convertion of G and [tz]G with GDA were performed the first-order reaction. From the curve fit in the KaleidaGraph, the initial rate constant (k) can be obtained and the reaction half-time ($t_{1/2}$) is calculated through following equations.

$$[A] = [A]_o e^{-kt}$$

$$t_{1/2} = \frac{\ln(2)}{k_1}$$

Where [A] is the experimental signal over time, $[A]_0$ is the initial signal at time zero, t is time, and k is the reaction rate coefficient. The coefficient of determination (R^2) for the curve fit were higher than 0.97 for the G and higher than 0.99 for [tz]G traces.
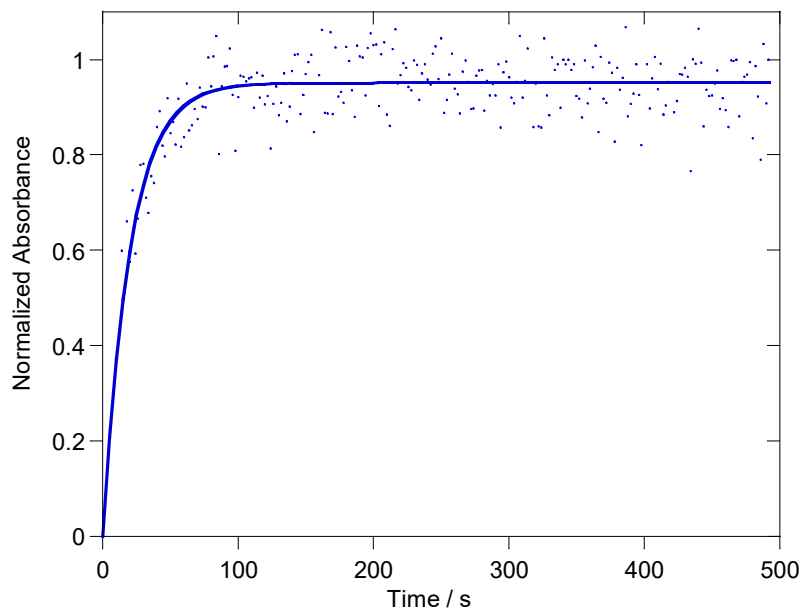
Graph 12. Kinetic absorbance spectrum of the enzymatic conversion of GDA with G
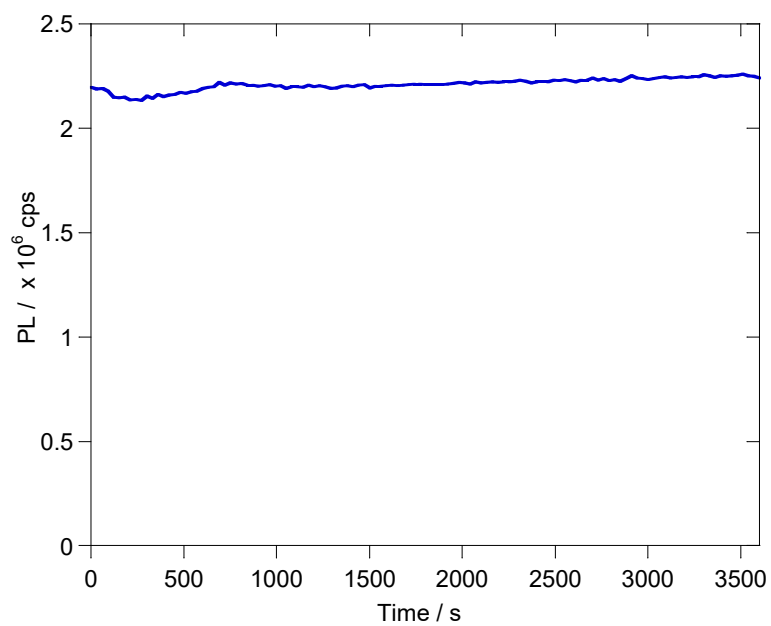
Graph 13. Kinetic emission spectrum of the enzymatic conversion of GDA with ᵗʰG

29

Graph 14. Kinetic emission spectrum of the enzymatic conversion of GDA with ^{tz}G
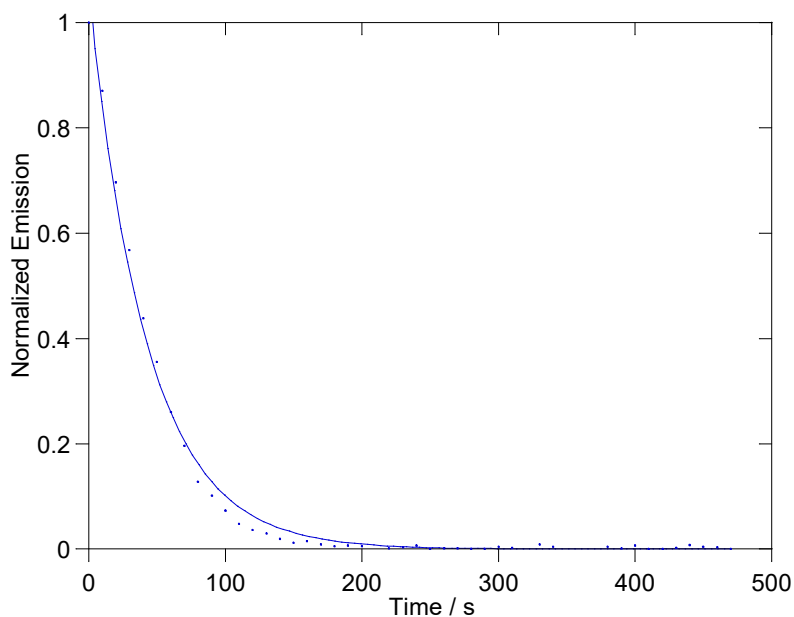
4.2.3. HPLC analysis for the enzymatic conversion

To further illustrate the results we got from last part, HPLC analysis was continued on a Agilent 1260 series system with an Eclipse XDB-C18, 5 μm, 4.6x150 mm column. The condition is same as used in kinetic analysis, while the concentration of nucleobases and enzyme is 2.00 μM and 2666 mU/ml in the solvent of phosphate buffer (50 mM, pH 7.5) and all samples reacted at 37.00±0.10°C. Formic acid is used to quench the reaction at 20, 40, 60, 80, 100, 200 and 500 seconds by mixing with the sample solution as the final concentration is 448 mM.[32- 38] The samples are then centrifuged at 3000g for 5 minutes and filtered to get the supernatant, which is put in ice bath before HPLC analysis. Each injection (40 μl) of G and ^{tz}G reactions was subjected to a gradient (15 minutes for the samples from G and ^{tz}G reaction and 17minutes for thG, from 0 to 95% of acetonitrile with 0.1% formic acid in water with 0.1% formic acid) followed by a flush (10 minutes). A flow rate of 1 ml / minute was used

and the run was carried out at 37.00 ± 0.10°C. Each run was monitored at 260, 280 and 320

nm with calibrated references at 600 nm and slit set at 1 nm (Graph 15, 17).

The HPLC traces were corrected for the blank and the concentration for each

component is calculated from the height (optical density) of the peaks. The concentration

changes were plotted as function of time. The trend line represents the loss of substrate (S)

and the product (P) formation for a first-order kinetic reaction according to the equation

bellow (Graph 16).

$$[S] = [S]_0\, e^{-k_1 t}$$

$$[P] = [P]_\infty\, (1 - e^{-k_1 t})$$
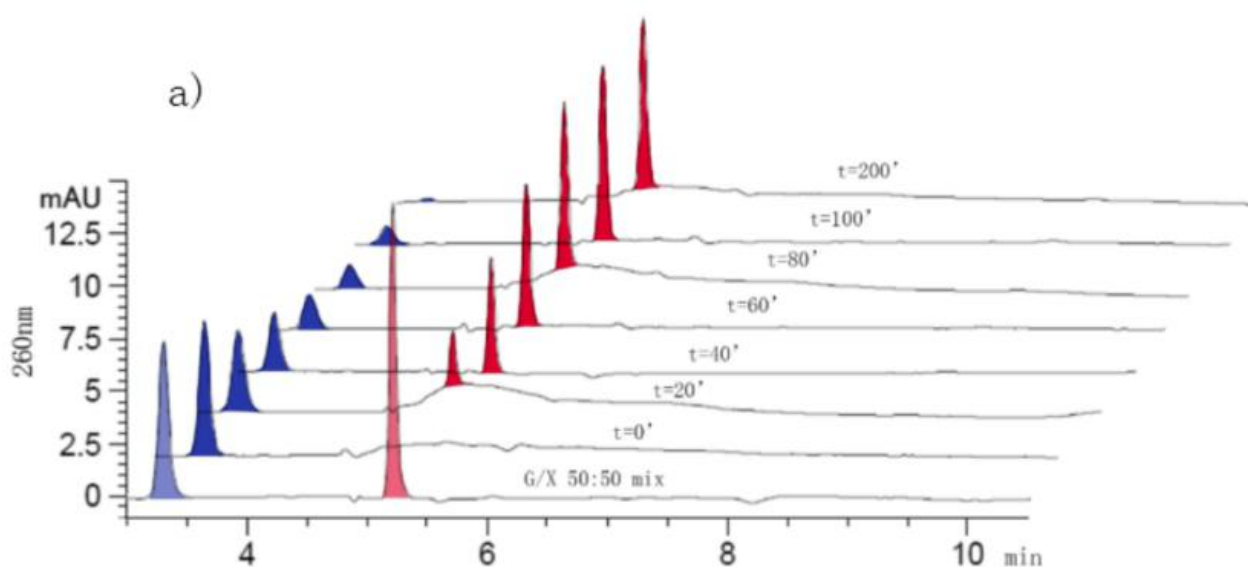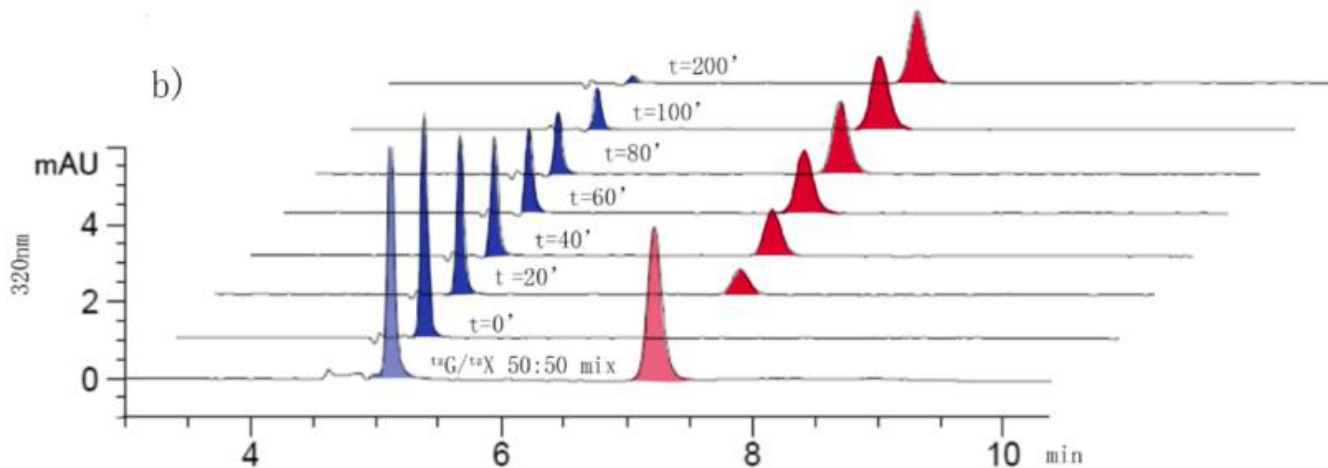
Graph 15. GDA-mediated deamination analysis by HPLC. Chromatogram showing the time course of enzymatic conversion of a) G to X b) ^{tz}G to ^{tz}X monitored at a) 260 nm b) 320 nm. Each set shows seven time points following the addition of ADA. For reference, an isomolar mixture of a) G and X b) ^{tz}G and ^{tz}X is shown at the bottom of each graph (transparent blue/red, respectively).
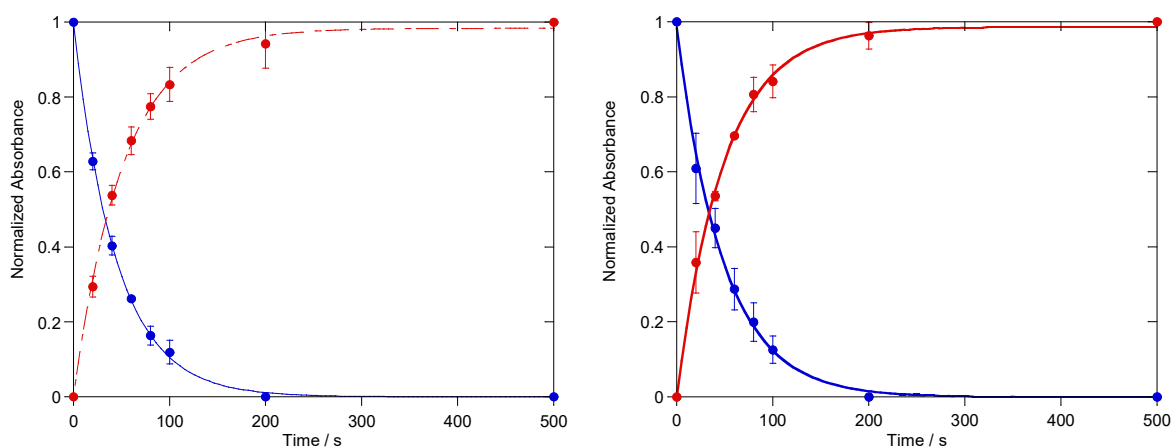
Graph 16. Trend line equations for the substrate consumption (solid red) and product formation (solid blue). Normalized absorbance versus time for G and ^{tz}G (red dots), X and ^{tz}X (blue dots) based on the HPLC traces.
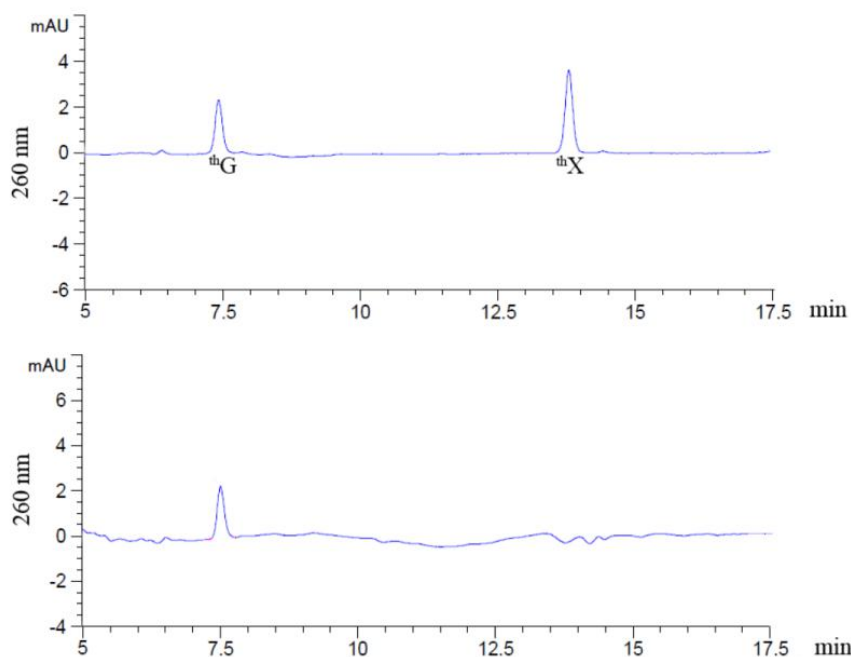
Graph 17. GDA-mediated deamination analysis for thG to thX by HPLC.

4.2.4. Activity of GDA after mixing with thG

The GDA-mediated deamination of G to X in the mixture of mixed GDA and thG was performed in the same condition of the individual deamination for HPLC analysis. Firstly, the GDA and thG is well-mixed and put in the incubator to maintain the temperature of 37°C, then the G is added into the mixture and the reaction is quenched by formic acid at 20s, 40s, 60s, 80s, 100s, 200s and 500s. After the same treatment we discussed before, the samples is analyzed by HPLC (Graph 18, 19).

Graph 18. GDA-mediated deamination analysis by HPLC of enzymatic conversion of G to X in the mixture of well mixed GDA and thG based on the 260 nm traces.For reference, an isomolar mixture of G, X, thG and thX is shown at the bottom of each graph (transparent blue/red/green/yellow, respectively).
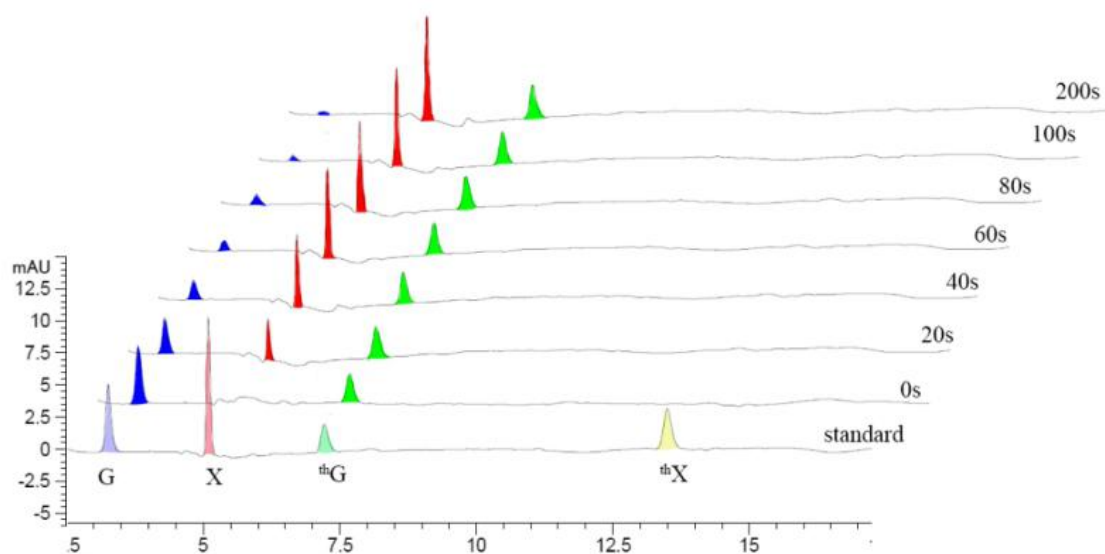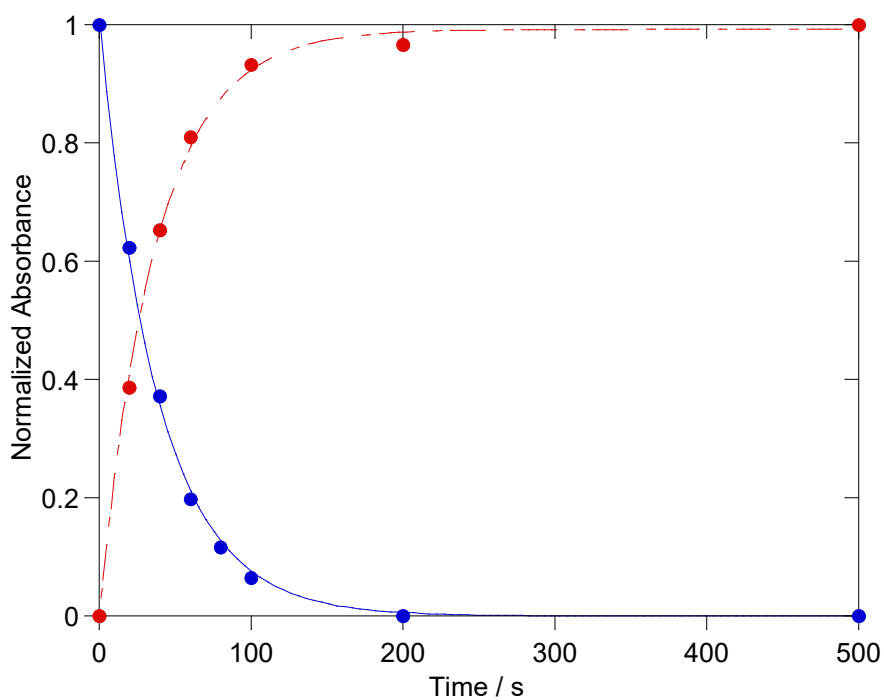

Graph 19. Trend line equations for the substrate consumption (solid red) and product formation (solid blue), Normalized absorbance versus time for G (red dots), X (blue dots) in the mixture of GDA and thG based on the HPLC traces at 260 nm.

5. Conclusion

In summary, the two emissive Guanine analogues (thG, ^{tz}G) and two xanthine analogues (thX, ^{tz}X), based on a thieno and isothiazole scaffold, respectively, were synthesized and characterized for their improved photophysical properties than native guanine and different biochemical activity due to the structural difference.

First of all, the crystal structure of these nucleobases analogues were measured to make sure the expected compound has been gotten. The result also proved the existence of tautomerization in the solid state of thG, which was also revealed by the convolution of emission spectra of thG. The similar H-bonding pattern of the analogues confirmed their structural analogy as the native nucleobases, makes them have the ability to be stabilized at the correct position of the active site of the enzyme. All of the nucleobases analogues possess fluorescence properties, illustrate by their emission spectra and sufficient quantum yield, which makes them a valuable surrogates of guanine. Their biochemical function was also tested by monitoring their activity with guanine deaminase (GDA), while the conversion of thienol guanine (thG) to thienol xanthine (thX) was barely catalyzed, however, the thiazole Guanine (^{tz}G) can react with GDA at the almost the same rate as the native guanine. This confirmed the significant role of N7 in the reaction since it's the biggest difference between thG and ^{tz}G. Furthermore, the unaffected activity of native guanine with the mixture of thG and GDA showed that thG is not an inhibitor in this specific concentration, which further proved that the thG cannot bind with GDA because of the absence of N7.

These observations about the novel guanine surrogates display improved structural and functional characteristics and help us better understand the binding and mechanism during the deamination process. What's more, a good fluorescent surrogate of guanine is provided, which facilitate a new fluorescence method to accurately and efficiently monitor the activity of GDA. Furthermore, help identify the inhibitor and activator to manipulate the activity of GDA, which is significant for the research of neurological recovery.

6. Additional information.

6.1. NMR Spectrum
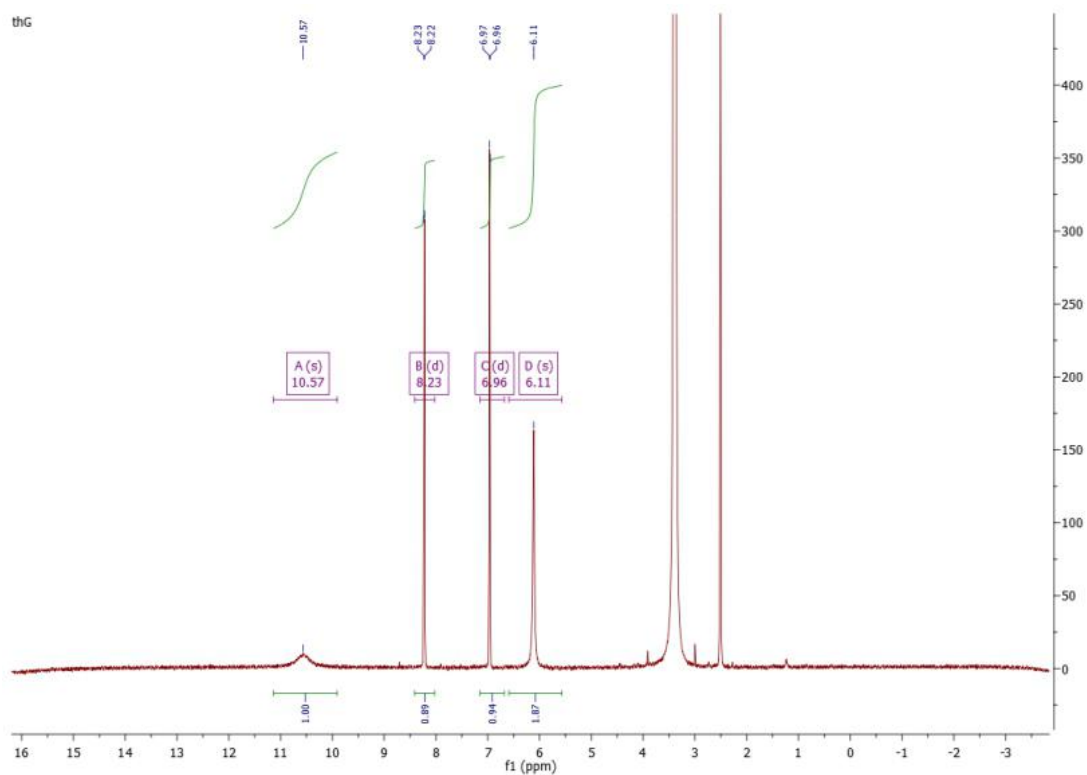
Figure 8. ^{1}H NMR of thG
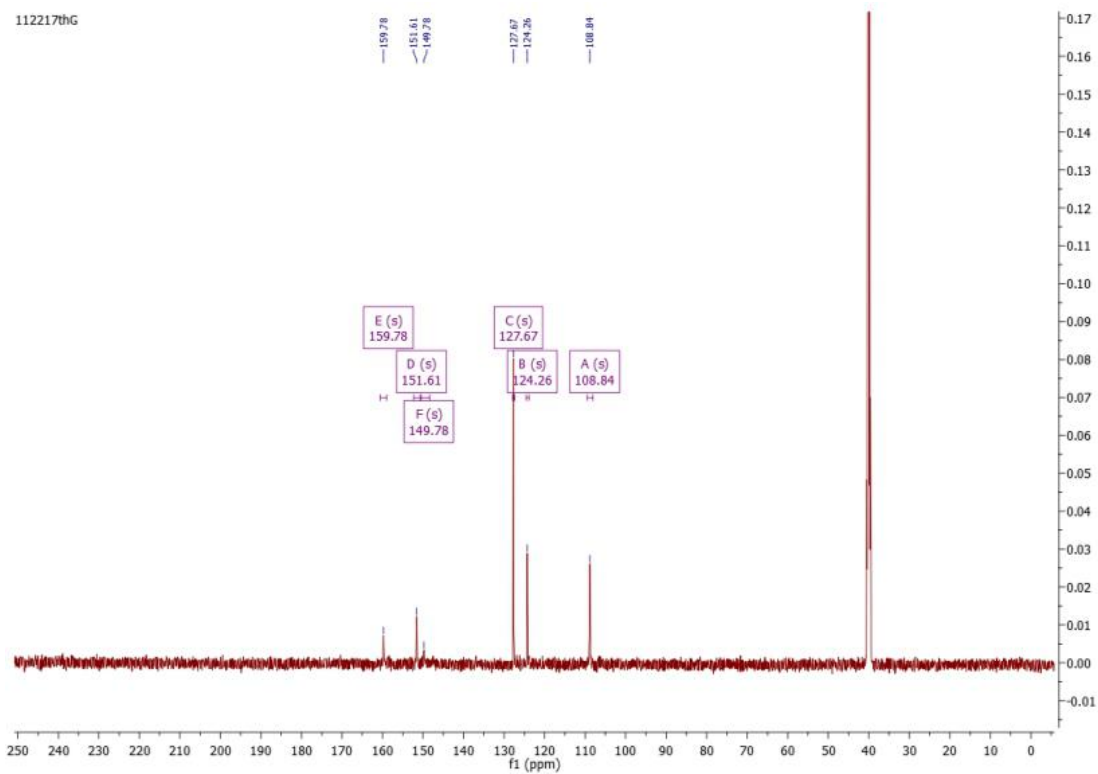
Figure 9. ^{13}C NMR of thG
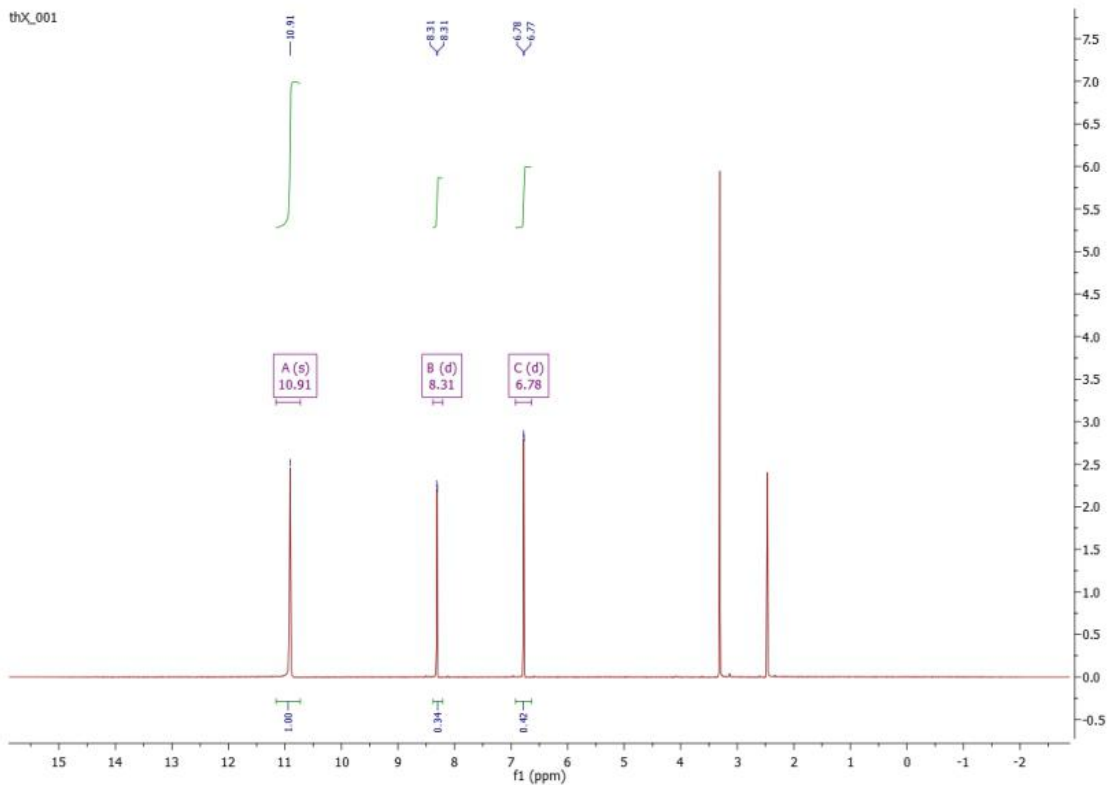
Figure 10. ^{1}H NMR of ^{th}X
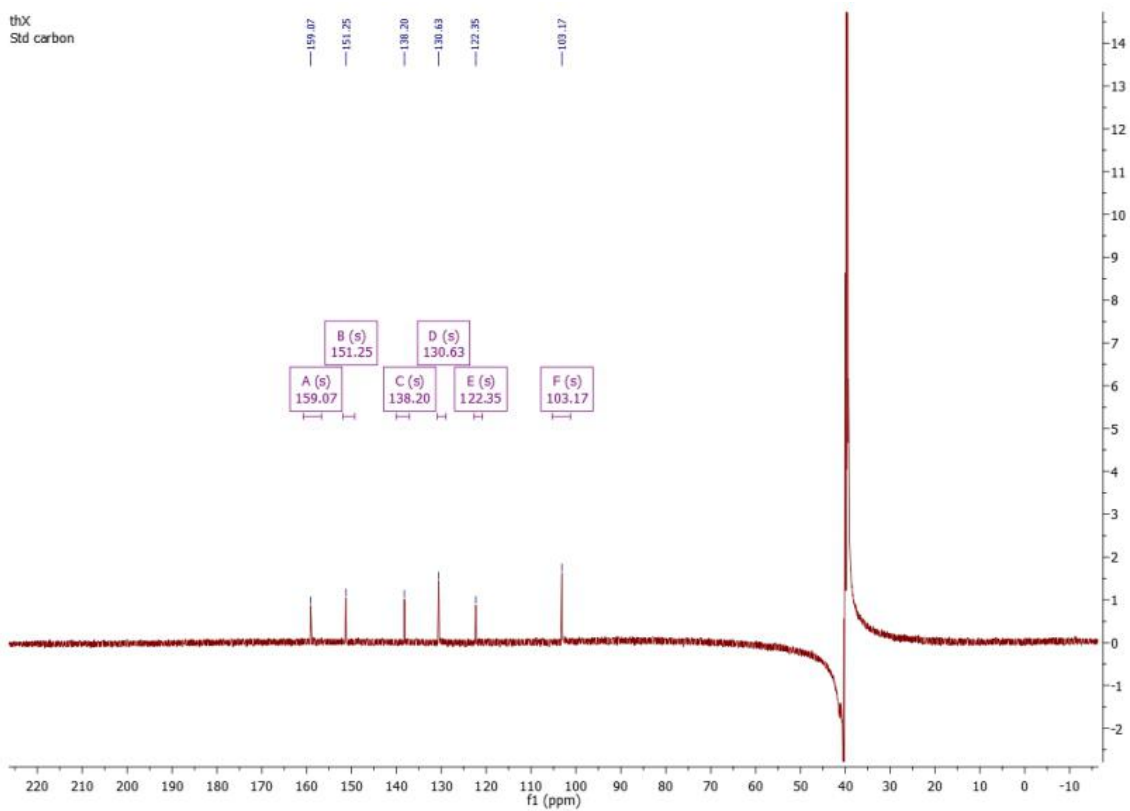
Figure 11. ^{13}C NMR of ^{th}X
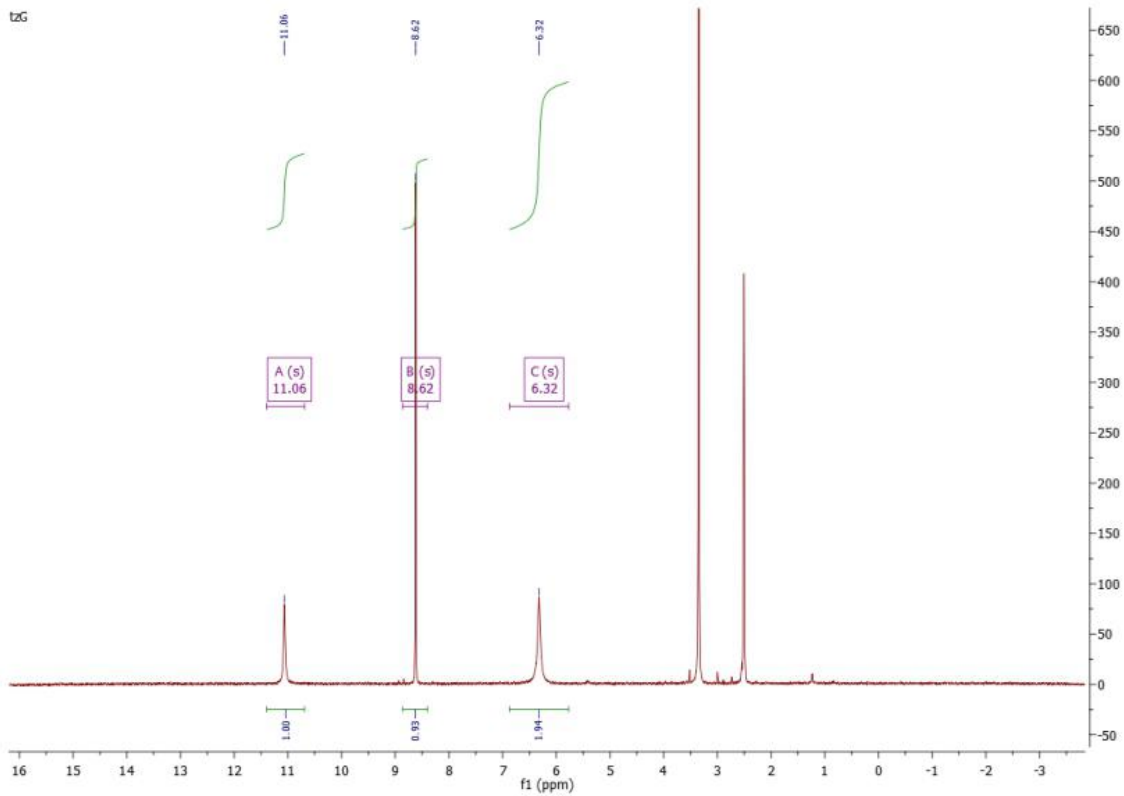
Figure 12. ^{1}H NMR of ^{tz}G
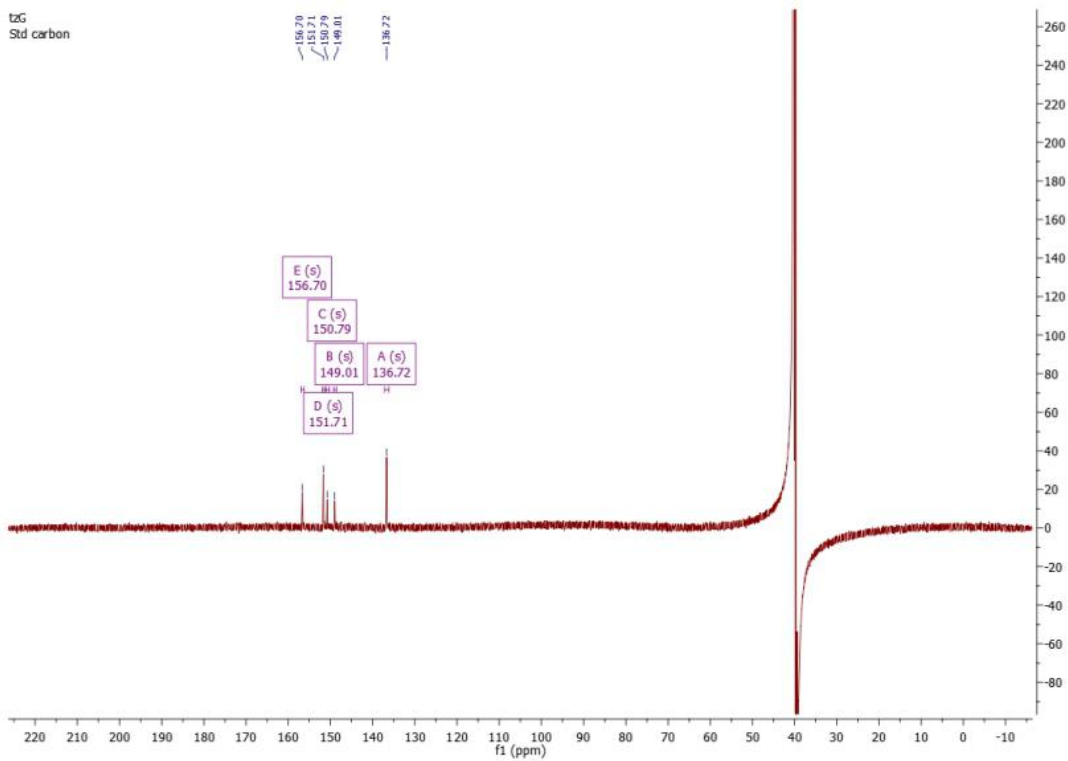
Figure 13. ^{13}C NMR of ^{tz}G
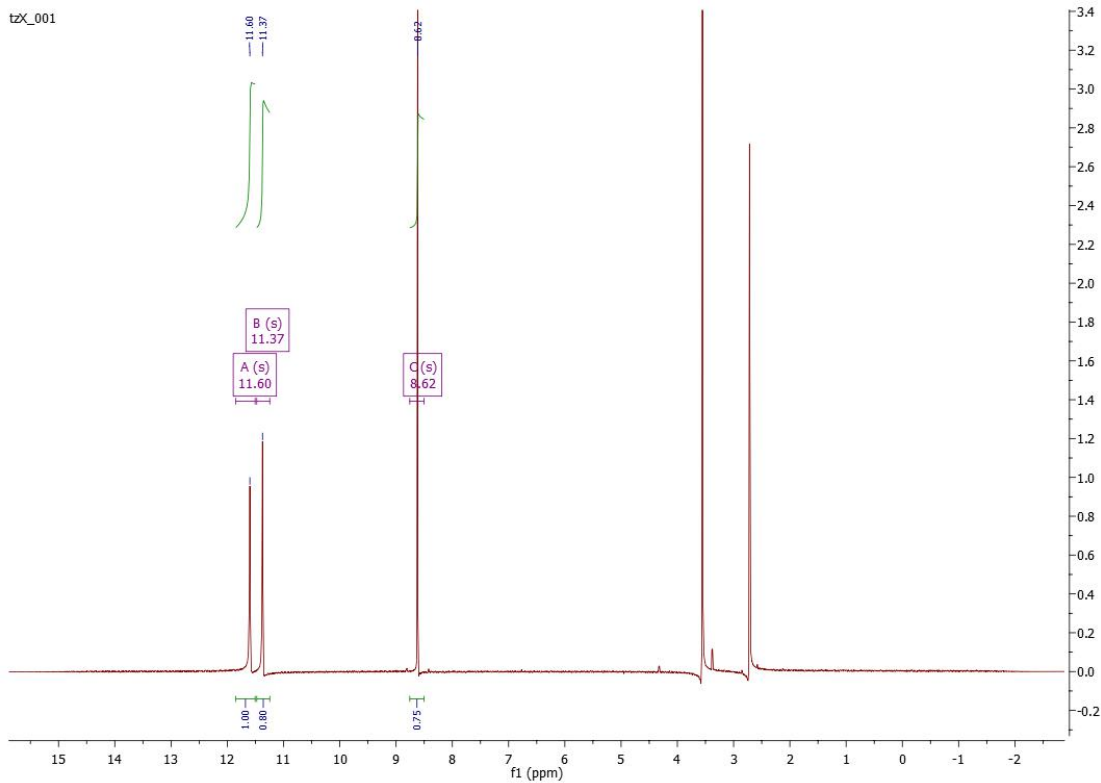
Figure 14. ^{1}H NMR of ^{tz}X
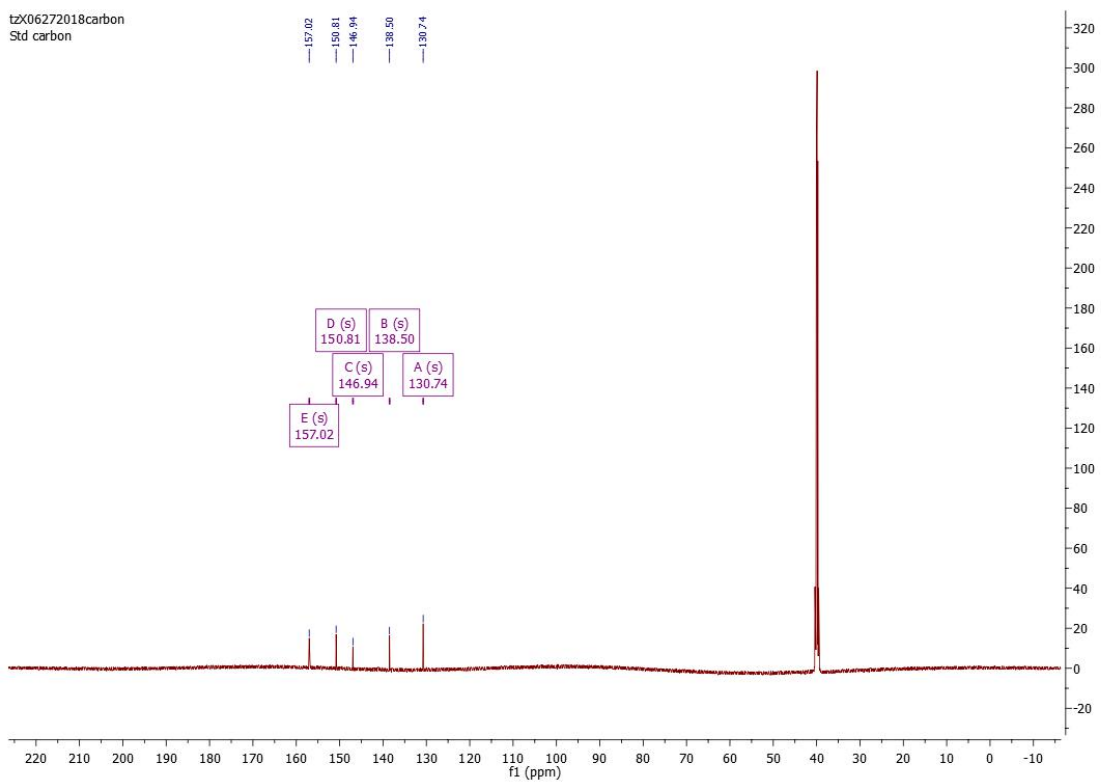
Figure 15. ^{13}C NMR of ^{tz}X

6.2. X-ray crystal structure

Table 3. Crystal data and structure refinement for thG.

Report date	2018-03-21
Identification code	thG
Empirical formula	C6 H5 N3 O S
Molecular formula	C6 H5 N3 O S
Formula weight	167.19
Temperature	100.0 K
Wavelength	1.54178 Å
Crystal system	Monoclinic
Space group	P 1 21/c 1

Unit cell dimensions

$a = 7.2425(6)$ Å $\quad = 90°.$

$b = 14.8279(12)$ Å $\quad = 94.751(3)°.$

$c = 12.8685(11)$ Å $\quad = 90°.$

Volume	1377.2(2) Å^3
Z	8
Density (calculated)	1.613 Mg/m^3
Absorption coefficient	3.680 mm^{-1}
F(000)	688
Crystal size	0.231 x 0.157 x 0.084 mm^3
Crystal color, habit	Colorless Block
Theta range for data collection	4.558 to 68.321°.
Index ranges	-8<=h<=8, -17<=k<=17, -15<=l<=14
Reflections collected	25913
Independent reflections	2519 [R(int) = 0.0310, R(sigma) = 0.0171]
Completeness to theta = 68.000°	99.8 %
Absorption correction	Semi-empirical from equivalents
Max. and min. transmission	0.3201 and 0.2149
Refinement method	Full-matrix least-squares on F^2
Data / restraints / parameters	2519 / 6 / 223
Goodness-of-fit on F^2	1.062
Final R indices [I>2sigma(I)]	R1 = 0.0301, wR2 = 0.0833
R indices (all data)	R1 = 0.0319, wR2 = 0.0849
Extinction coefficient	n/a
Largest diff. peak and hole	0.256 and -0.267 e.Å^{-3}
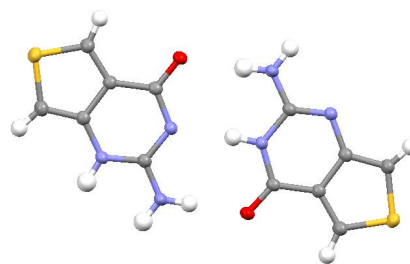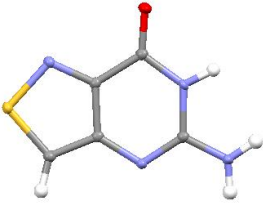
Table 4. Crystal data and structure refinement for ᵗʰX.

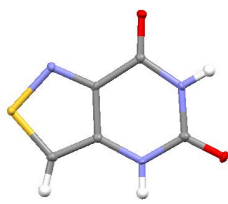|	
Report date	2018-04-04
Identification code	THX01
Empirical formula	C6 H4 N2 O2 S
Molecular formula	C6 H4 N2 O2 S
Formula weight	168.17
Temperature	100.0 K
Wavelength	0.71073 Å
Crystal system	Monoclinic
Space group	P 1 21/c 1
Unit cell dimensions	a = 10.1968(16) Å $\quad$ = 90°.
	b = 5.3149(8) Å $\quad$ = 102.119(4)°.
	c = 12.257(2) Å $\quad$ = 90°.
Volume	649.48(18) Å³
Z	4
Density (calculated)	1.720 Mg/m³
Absorption coefficient	0.436 mm⁻¹
F(000)	344
Crystal size	0.271 x 0.117 x 0.093 mm³
Crystal color, habit	Colorless Block
Theta range for data collection	2.043 to 28.278°.
Index ranges	-13<=h<=13, -6<=k<=7, -16<=l<=13
Reflections collected	8784
Independent reflections	1596 [R(int) = 0.0582, R(sigma) = 0.0463]
Completeness to theta = 25.000°	100.0 %
Absorption correction	Semi-empirical from equivalents
Max. and min. transmission	0.2482 and 0.2096
Refinement method	Full-matrix least-squares on F²
Data / restraints / parameters	1596 / 2 / 108
Goodness-of-fit on F²	1.075
Final R indices [I>2sigma(I)]	R1 = 0.0376, wR2 = 0.0963
R indices (all data)	R1 = 0.0435, wR2 = 0.1004
Extinction coefficient	n/a
Largest diff. peak and hole	0.361 and -0.331 e.Å⁻³
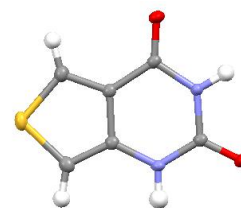
Table 5. Crystal data and structure refinement for ᵗᶻG.

Report date	2018-07-10	
Identification code	tor119	
Empirical formula	C5 H4 N4 O S	
Molecular formula	C5 H4 N4 O S	
Formula weight	168.18	
Temperature	100.0 K	
Wavelength	0.71073 Å	
Crystal system	Monoclinic	
Space group	P 1 21/c 1	
Unit cell dimensions	a = 3.6599(2) Å	$\alpha = 90°$.
	b = 11.2567(5) Å	$\beta = 96.825(2)°$.
	c = 15.0364(7) Å	$\gamma = 90°$.
Volume	615.09(5) Å^3	
Z	4	
Density (calculated)	1.816 Mg/m^3	
Absorption coefficient	0.457 mm^{-1}	
F(000)	344	
Crystal size	0.03 x 0.005 x 0.005 mm^3	
Crystal color, habit	light yellow needle	
Theta range for data collection	2.266 to 26.720°.	
Index ranges	-4<=h<=4, -13<=k<=14, -18<=l<=18	
Reflections collected	9691	
Independent reflections	1303 [R(int) = 0.0555]	
Completeness to theta = 25.242°	100.0 %	
Absorption correction	Semi-empirical from equivalents	
Max. and min. transmission	0.7455 and 0.6591	
Refinement method	Full-matrix least-squares on F^2	
Data / restraints / parameters	1303 / 0 / 100	
Goodness-of-fit on F^2	1.046	
Final R indices [I>2sigma(I)]	R1 = 0.0337, wR2 = 0.0733	
R indices (all data)	R1 = 0.0471, wR2 = 0.0784	
Largest diff. peak and hole	0.332 and -0.314 e.Å^{-3}	

Table 6. Crystal data and structure refinement for ^{tz}X.

Report date	2018-07-11
Identification code	tor120
Empirical formula	C5 H3 N3 O2 S
Molecular formula	C5 H3 N3 O2 S
Formula weight	169.16
Temperature	100.0 K
Wavelength	0.71073 Å
Crystal system	Monoclinic
Space group	P 1 21/c 1
Unit cell dimensions	a = 6.9522(10) Å $\qquad$ α= 90°.
	b = 12.2384(17) Å $\qquad$ β= 93.431(3)°.
	c = 6.9021(10) Å $\qquad$ γ = 90°.
Volume	586.20(14) Å^3
Z	4
Density (calculated)	1.917 Mg/m^3
Absorption coefficient	0.488 mm^{-1}
F(000)	344
Crystal size	0.12 x 0.08 x 0.04 mm^3
Crystal color, habit	colorless block
Theta range for data collection	2.935 to 26.736°.
Index ranges	-8<=h<=8, 0<=k<=15, 0<=l<=8
Reflections collected	1244
Independent reflections	1244 [R(int) = 0.0362]
Completeness to theta = 25.242°	100.0 %
Absorption correction	Semi-empirical from equivalents
Max. and min. transmission	0.491 and 0.402
Refinement method	Full-matrix least-squares on F^2
Data / restraints / parameters	1244 / 0 / 101
Goodness-of-fit on F^2	1.036
Final R indices [I>2sigma(I)]	R1 = 0.0362, wR2 = 0.0873
R indices (all data)	R1 = 0.0456, wR2 = 0.0927
Largest diff. peak and hole	0.409 and -0.459 e.Å^{-3}

6.3. Raw HPLC Traces
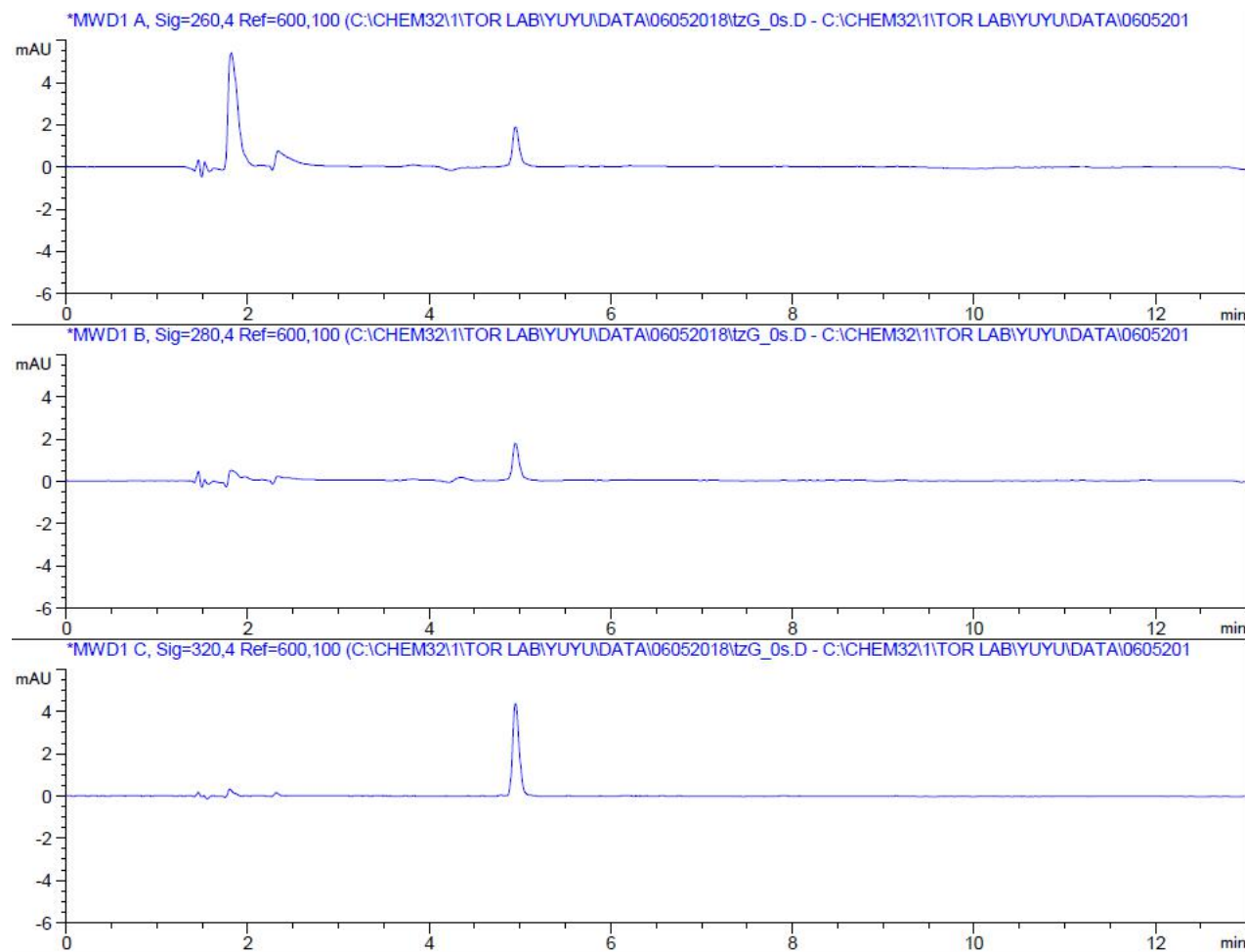
Figure 16. GDA-mediated ^{tz}G to ^{tz}X conversion at t = 0 s.
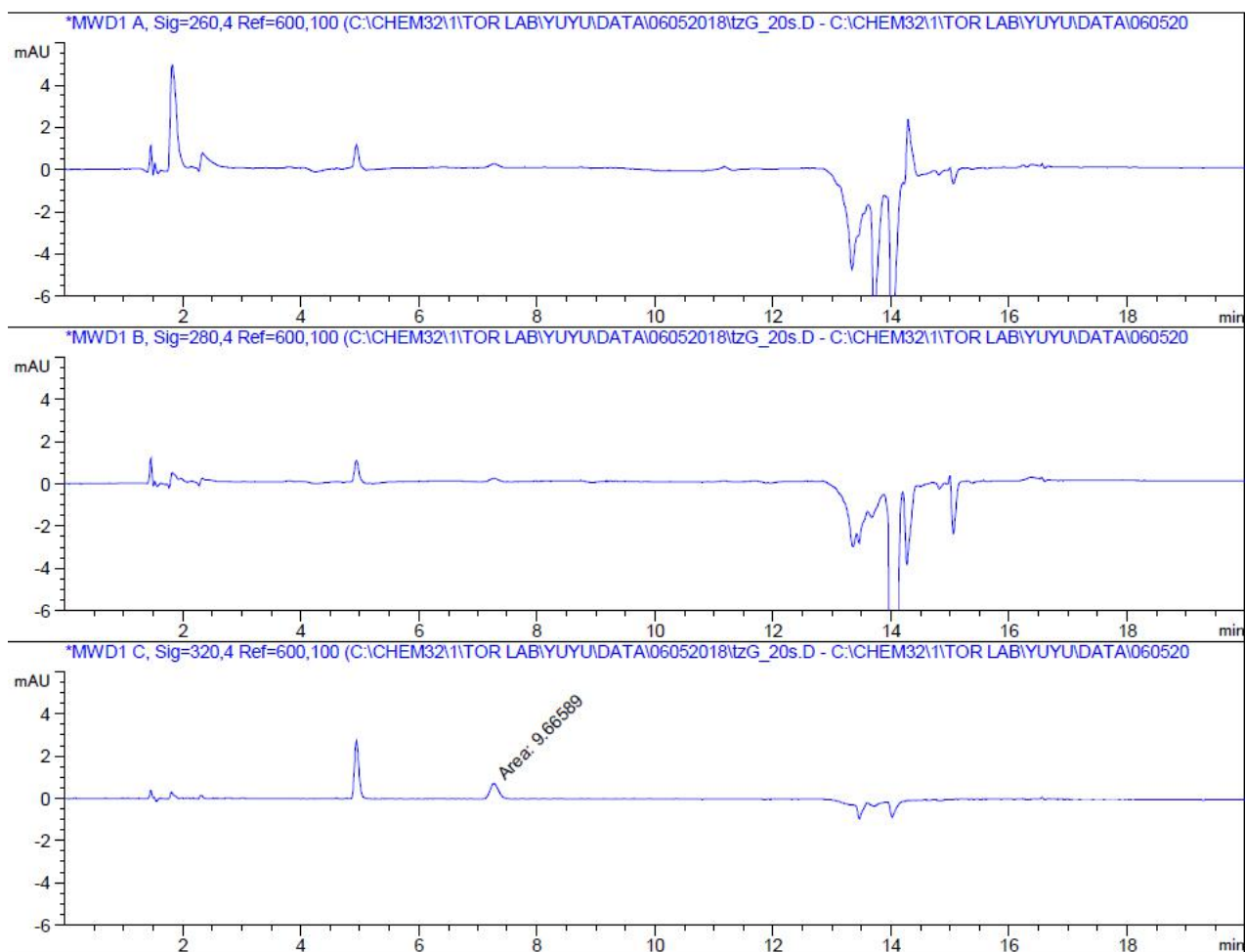
Figure 17. GDA-mediated ^{tz}G to ^{tz}X conversion at t = 20 s.

46
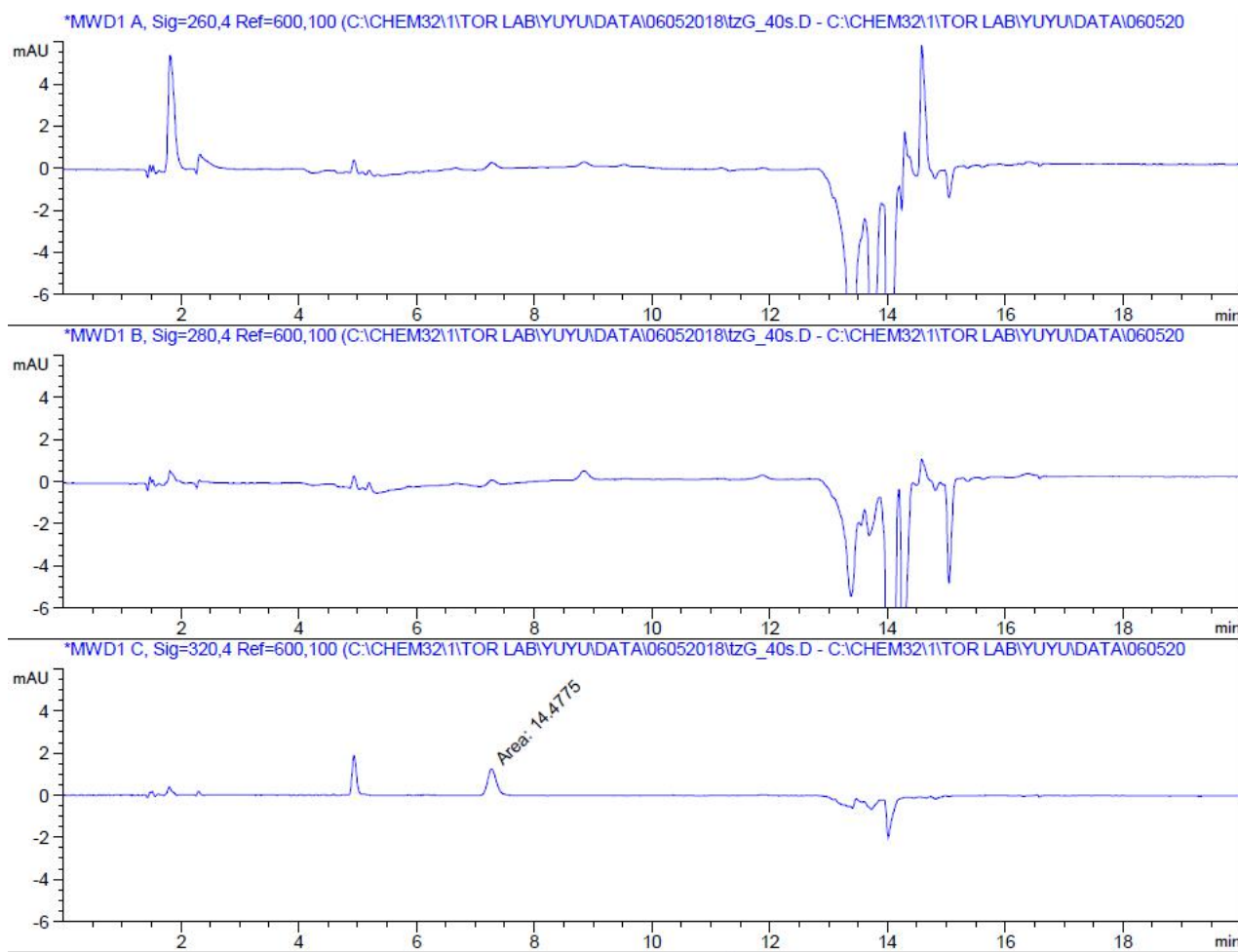
Figure 18. GDA-mediated ^{tz}G to ^{tz}X conversion at t = 40 s.
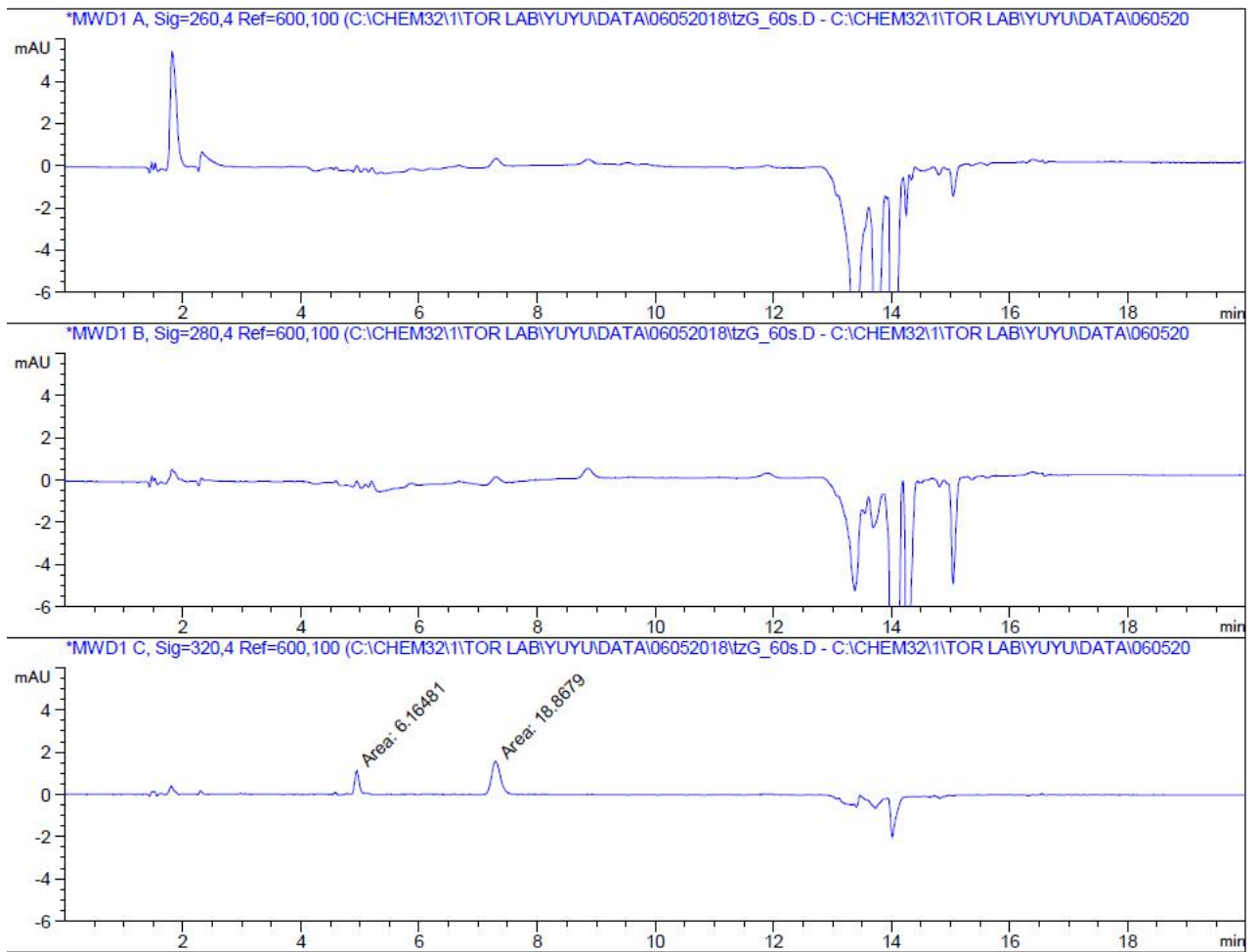
Figure 19. GDA-mediated ^{tz}G to ^{tz}X conversion at t = 60 s.
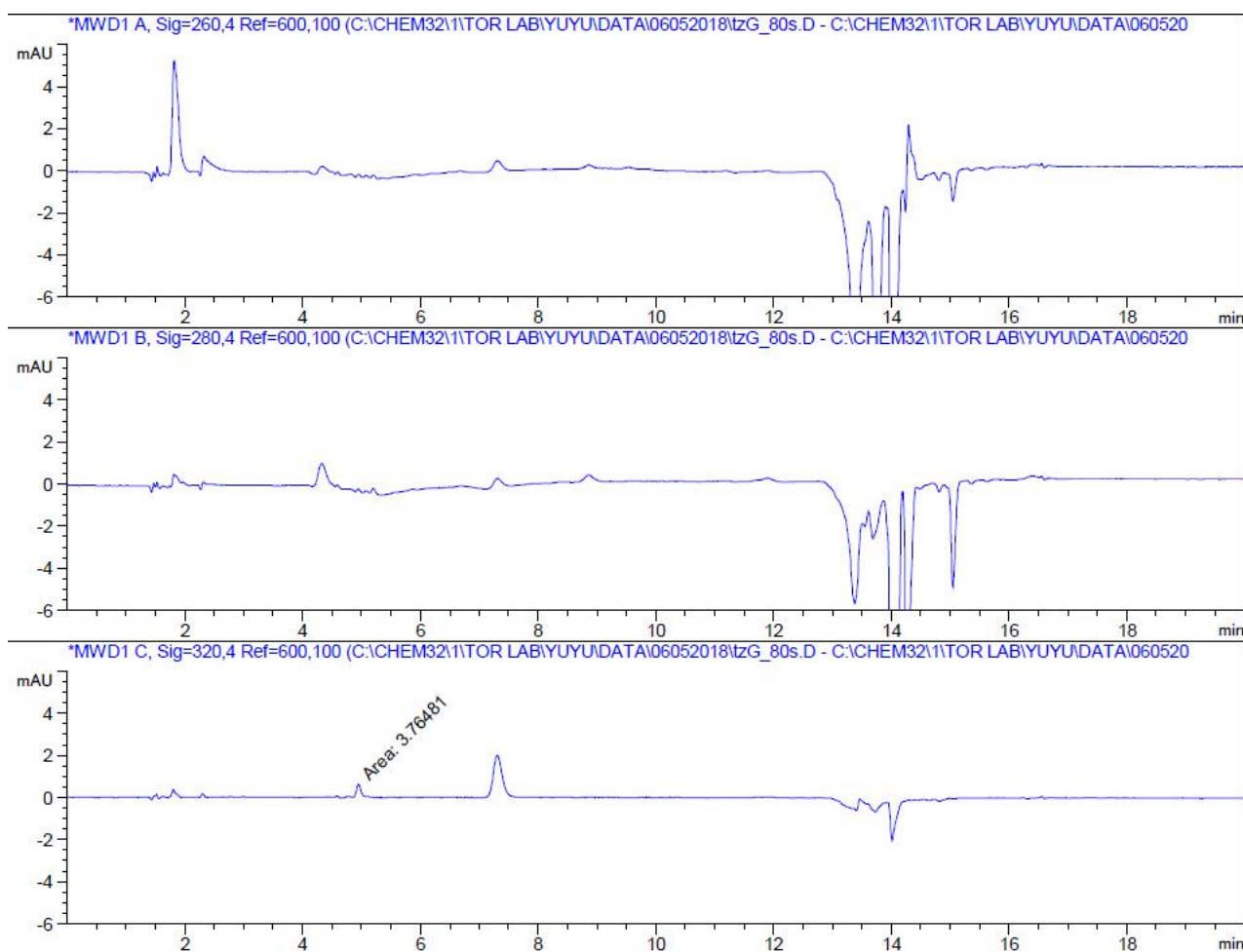
Figure 20. GDA-mediated ^{tz}G to ^{tz}X conversion at t = 80 s.
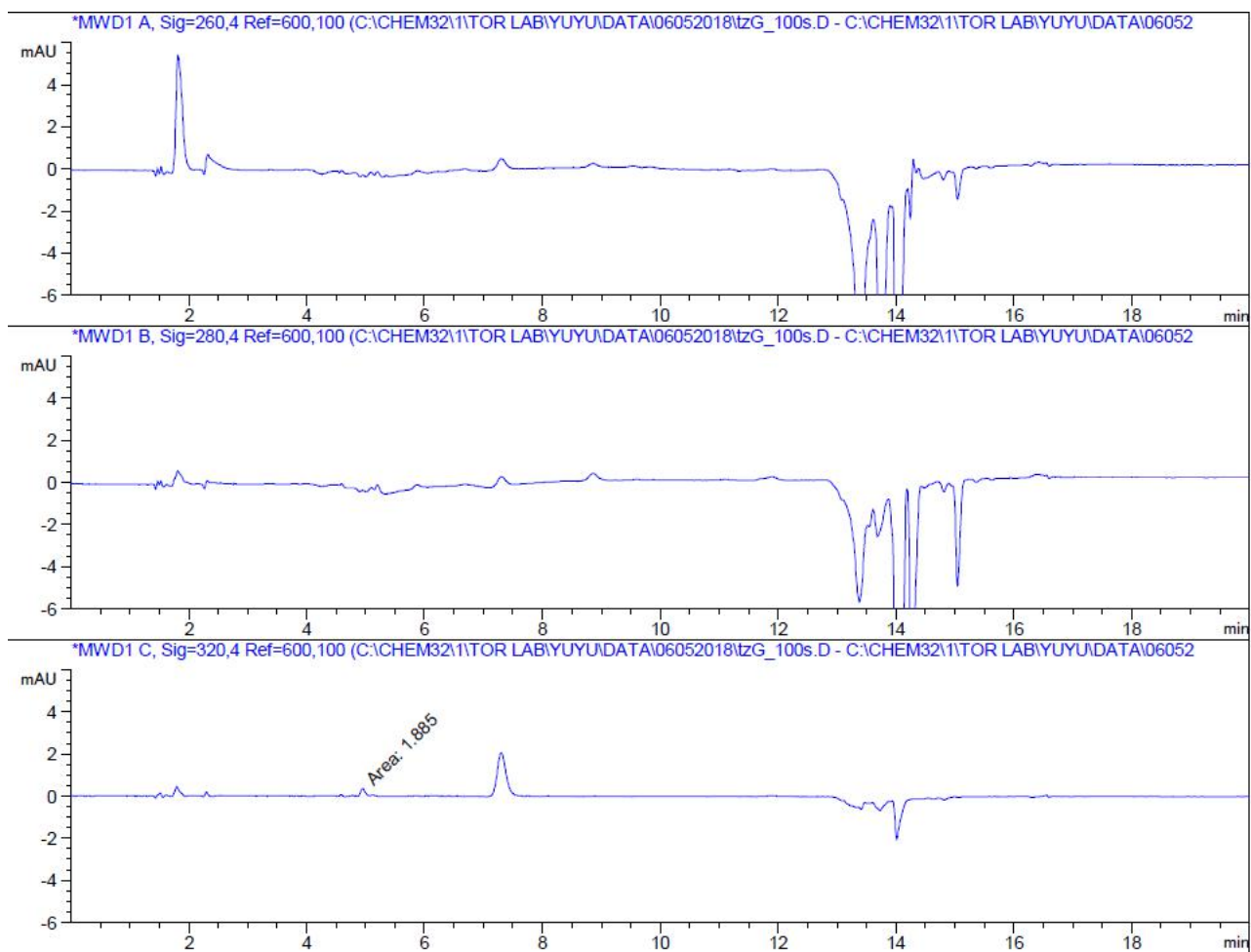
Figure 21. GDA-mediated ^{tz}G to ^{tz}X conversion at t = 100 s.
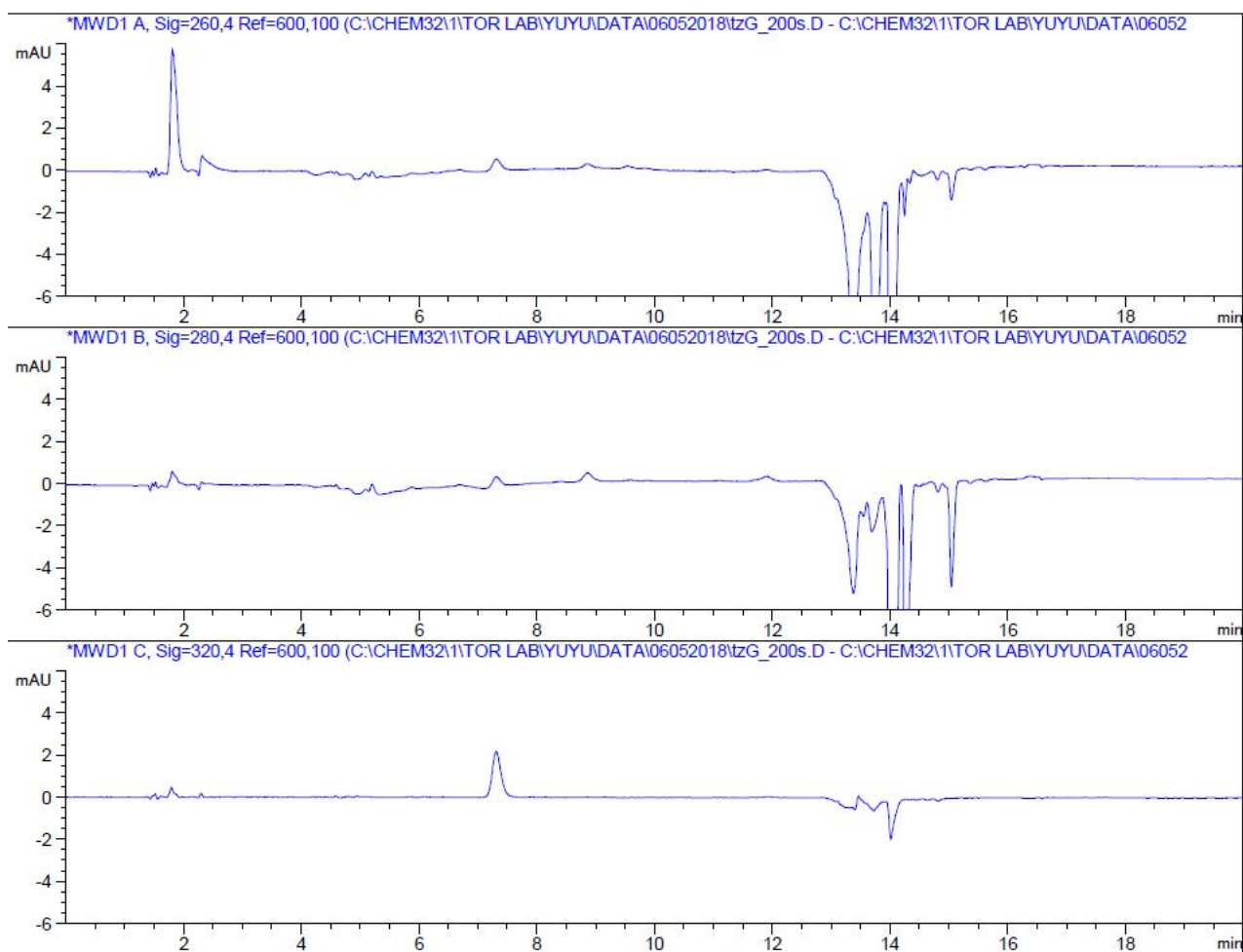
Figure 22. GDA-mediated ^{tz}G to ^{tz}X conversion at t = 200 s.

Figure 23. GDA-mediated ^{tz}G to ^{tz}X conversion at t = 500 s.

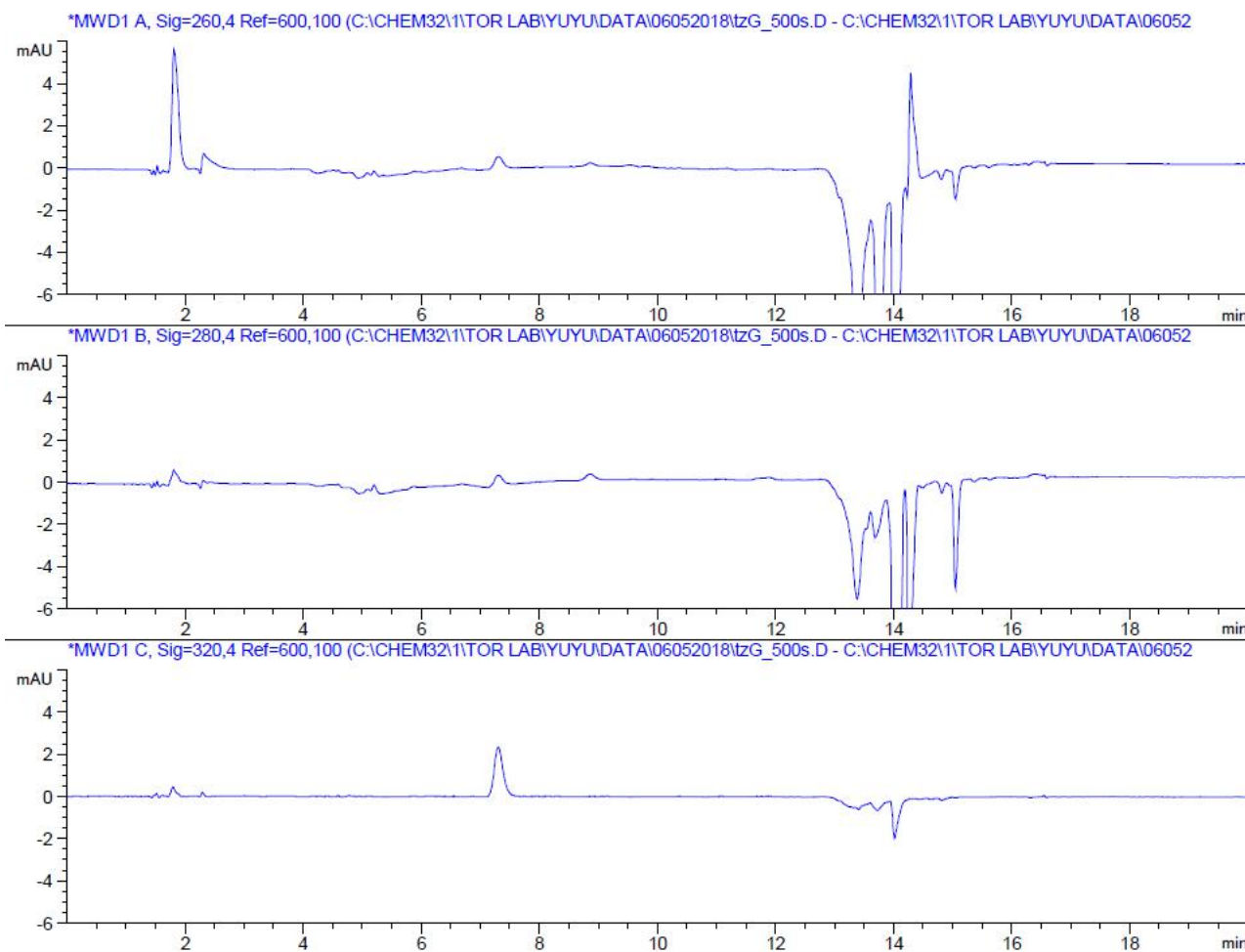## References

1. Hitchings, G. H.; Falco, E. A. "The Identification of Guanine in Extracts of Girella Nigricans: The Specificity of Guanase". *Proceedings of the National Academy of Sciences of the United States of America.* Oct 1944. 30 (10): 294–7. doi:10.1073/pnas.30.10.294. PMC 1078714 Freely accessible. PMID 16578130.

2. Kalckar, H. M. "Differential spectrophotometry of purine compounds by means of specific enzymes; studies of the enzymes of purine metabolism". *J. Biol. Chem.* 1947. 167 (2): 461–75. PMID 20285041.

3. Rabinowitz, J. C.; Barker, H. A. "Purine fermentation by Clostridium cylindrosporum. II. Purine transformations". *The Journal of Biological Chemistry.* Jan 1956. 218 (1): 161–73. PMID 13278325.

4. Swiatkowski, P.; Sewell, E.; Sweet E. S.; Dickson, S.; Swanson, R. A.; McEwan, S. A.; Cuccolo, N.; McDonnell, M. E.; Patel, M. V.; Varghese, N.; Morrison, B.; Reitz, A. B.; Meaney, D. F.; Firestein, B. L. "Cypin: A novel target for traumatic brain injury" *Neurobiology of Disease* 119 (2018) 13–25.

5. Kumar, S., Rathi, M. "Deficiency of a naturally occurring protein inhibitor in brain of clinically 'brain damaged' newborn human infants - a possible cause of mental retardation?" *Neurosci. Lett.* 1976. 3, 163–165.

6. Kumar, S., Ou, S.W., Rathi, M. "Deficiency of guanine deaminase in human brain: a new brain disorder?" *N. Engl. J. Med.* 1979. 300, 1332–1333.

7. Adams, S.M., et al. "ABCG2 c.421C>A is associated with outcomes after severe traumatic brain injury." *J. Neurotrauma*. 2018. 35, 48–53.

8. Hatefi, M., Dastjerdi, M.M., Ghiasi, B., Rahmani, A. "Association of Serum Uric Acid Level with the severity of brain injury and Patient's outcome in severe traumatic brain injury." *J. Clin. Diagn. Res.* 2016. 10, OC20–OC24.

9. Akum, B. F.; Chen, M.; Gunderson, S. I.; Riefler, G. M.; Scerri-Hansen, M. M.; Firestein, B. L. "Cypin regulates dendrite patterning in hippocampal neurons by promoting microtubule assembly." *Nat. Neurosci.* 7, 2004, 145–152.

10. Patel, M.V.; Swiatkowski, P.; Kwon, M.; Rodriguez, A. R.; Campagno, K.; Firestein, B. L. "A novel short isoform of cytosolic PSD-95 interactor (Cypin) regulates neuronal development." *Mol. Neurobiol.* 55 (8), 2018, 6269–6281.

11. Campbell, J.N.; Low, B.; Kurz, J. E.; Patel, S. S.; Young, M. T.; Churn, S. B.

"Mechanisms of dendritic spine remodeling in a rat model of traumatic brain injury." *J. Neurotrauma.* 2012. 29, 218–234.

12. Fernández, J. R.; Sweet, E. S.; Welsh, W. J.; Firestein, B. L; "Identification of small molecule compounds with higher binding affinity to guanine deaminase (cypin) than guanine" *Bioorganic & Medicinal Chemistry* 18 (2010) 6748–6755.

13. Bitra, A.; Biswas, A.; Anand, R. "Structural Basis of the Substrate Specificity of Cytidine Deaminase Superfamily Guanine Deaminase" *Biochemistry* 2013, 52, 8106−8114.

14. Sinkeldam, R. W.; Greco, N.J.; Tor, y. "Fluorescent Analogs of Biomolecular Building Blocks: Design, Properties, and Applications." *Chem. Rev.* 2010, 110, 2579–2619.

15. Bitra, A.; Hussain, B.; Tanwar, A. S.; Anand, R. "Identification of Function and Mechanistic Insights of Guanine Deaminase from Nitrosomonas europaea: Role of the C− Terminal Loop in Catalysis" *Biochemistry* 2013, 52, 3512−3522.

16. Hall, R. S.; Fedorov,A. A.; Marti-Arbona, R.; Fedorov, E. V.; Kolb, P.; Sauder, J. M.;| Burley, S. K.; Shoichet, B. K.; Almo, S. C.; Raushel, F. M. "The Hunt for 8-Oxoguanine Deaminase" *J. AM. CHEM. SOC.* 2010, 132, 1762–1763.

17. Kumaran, D., Burley, S.K., Swaminathan, S., New York SGX Research Center for Structural Genomics (NYSGXRC) (PDB entry 2I9U)

18. Liaw, S. H.; Chang, Y.; Lai, C.; Chang, H.; Chang, G. "Crystal Structure of Bacillus subtilis Guanine Deaminase" *THE JOURNAL OF BIOLOGICAL CHEMISTRY*, 2004, DOI 10.1074/jbc.M405304200.

19. Shin, D.; Sinkeldam, R. W.; Tor, Y. "Emissive RNA Alphabet" *J. Am. Chem. Soc.* **2011**, *133*, 14912-14915.

20. Shah, R.; Zhou, A.; Wagner, C. R. "Switch-on fluorescent/FRET probes to study human histidine triad nucleotide binding protein 1 (hHint1), a novel target for opioid tolerance and neuropathic pain" *Organic and Biomolecular Chemistry*, 2017, vol. 15, #48, p. 10230 - 10237.

21. Venskutonyte, R.; Butini, S.; Coccone, S. S.; Gemma, S.; Brindisi, M.; Kumar, V.; Guarino, E.; Maramai, S.; Valenti, S.; Ahmad, A.; Valadés, E. A.; Frydenvang, K.; Kastrup, J. S.; Novellino, E.; Campiani, G.; Pickering, D. S. "Selective Kainate Receptor (GluK1) Ligands Structurally Based upon 1H-Cyclopentapyrimidin-2,4(1H,3H)-dione: Synthesis, Molecular Modeling, and Pharmacological and Biostructural Characterization" *Journal of Medicinal Chemistry*, 2011, vol. 54, # 13, p. 4793 - 4805

22. Srivatsan, S. G.; Weizman, H.; Tor, Y. "A highly fluorescent nucleoside analog based on thieno[3,4-d] pyrimidine senses mismatched pairing" *Organic and Biomolecular Chemistry,* 2008, vol. 6, # 8, p. 1334 - 1338

23. Rovira, A. R.; Fin, A.; Tor, Y. "Expanding a fluorescent RNA alphabet: synthesis, photophysics and utility of isothiazole-derived purine nucleoside surrogates" *Chem. Sci.* **2017,** *8*, 2983-2993.

24. Chakraborty, S.; Shah, N. H.; Fishbein, J. C.; Hosmane, R. S. "Investigations into specificity of azepinomycin for inhibition of guanase: Discrimination between the natural heterocyclic inhibitor and its synthetic nucleoside analogues" *Bioorganic & Medicinal Chemistry Letters* 22 (2012) 7214–7218.

25. Sholokh, M.; Sharma, R.; Shin, D.; Tor, Y.; Mely, Y. "Conquering 2-Aminopurine's Deficiencies: Highly Emissive Isomor-phic Guanosine Surrogate Faithfully Monitors Guanosine Conformation and Dynamics in DNA" *J. Am. Chem. Soc.* **2015**, *137*, 3185-3188.

26. Shin, D. S.; Lonn, P.; Dowdy, S. F.; Tor, Y. "Cellular activity of siRNA oligonucleotides containing synthetic isomorphic nucleosidesurrogates" *Chem. Commun.*, 2015, 51, 1662--1665.

27. Sinkeldam, R. W.; McCoy, L. S.; Shin, D.; Tor, Y. "Enzymatic Interconversion of Isomorphic Fluorescent Nucleosides: Adenosine Deaminase Transforms an Adenosine Analogue into an Inosine Analogue" *Angew. Chem. Int. Ed.* **2013**, *52*, 14026-14030.

28. Mizrahi, R. A.; Shin, D.; Sinkeldam, R. W.; Phelps, K. J.; Fin, A.; Tantillo, D. J.; Tor, Y; Beal, P. A. "A Fluorescent Adenosine Analogue as a Substrate for an A-to-I RNA Editing Enzyme" *Angew. Chem. Int. Ed.* **2015**, *54*, 8713-8716.

29. Rovira, A. R.; Fin, A.; Tor, Y. "Chemical Mutagenesis of an Emissive RNA Alphabet" *J. Am. Chem. Soc.* **2015,** *137*, 14602-14605.

30. Sholokh, M.; Improta, R.; Mori, M.; Sharma, R.; Kenfack, C.; Shin, D.; Voltz, K.; Stote, R. H.; Zaporozhets, O. A.; Botta, M.; Tor, Y.; Mely, Y. "Tautomers of a Fluorescent G Surrogate and Their Distinct Photophysics Provide Additional Information Channels" *Angew. Chem. Int. Ed*. 2016, 55, 7974 –7978

31. Millen, A. L.; Churchill, C. D. M.; Manderville, R. A.; Wetmore, S. D. "Effect of Watson-Crick and Hoogsteen Base Pairing on the Conformational Stability of C8-Phenoxyl-2′-deoxyguanosine Adducts" *J. Phys. Chem.* B 2010, 114, 12995–13004

32. Paul, M. K.; Grover, V.; Mukhopadhyay, A. K. "Merits of HPLC-based method over spectrophotometric method for assessing the kinetics and inhibition of mammalian adenosine

deaminase" *Journal of Chromatography B*, 822 (2005) 146–153.

33. Roberts, E. L. L.; Newton, R. P. "Estimation of guanine deaminase using guanosine as a 'prosubstrate'." *Analytical Biochemistry* 324 (2004) 250–257

34. Negishi, O.; Ozawa, T.; Imagawa, H. "Guanosine Deaminase and Guanine Deaminase from Tea Leaves." *Biosci. Biotech. Biochem.*, 58 (7), 1277 1281, 1994

35. Canepari, S.; Carunchio, V.; Girelli, A. M.; Messina, A. "New method for guanase activity measurement by high-performance liquid chromatography." *Journal of Chromatography*, 616 (1993) 25-30

36. Nolan, L. L. "Partial Purification and Characterization of Guanine Aminohydrolase from Trypanosoma cruzi" *CURRENT MICROBIOLOGY*, Vol. 11 (1984), pp. 217-220.

37. Kim, J.; Park, S. I.; Ahn, C.; Kim, H.; Yim, J. "Guanine Deaminase Functions as Dihydropterin Deaminase in the Biosynthesis of Aurodrosopterin, a Minor Red Eye Pigment of Drosophila." *THE JOURNAL OF BIOLOGICAL CHEMISTRY* VOL. 284, NO. 35, pp. 23426–23435.

38. Wilson, D. K.; Quiocho, F. A. "A Pre-Transition-State Mimic of an Enzyme: X-ray Structure of Adenosine Deaminase with Bound 1-Deazaadenosine and Zinc-Activated Water" *American Chemical Society*, 1993, 0006-2960/93/0432-1689.